Impact of changes in climate and CO_2 on the carbon storage potential of vegetation under limited water availability using SEIB-DGVM version 3.02

Shanlin Tong[1,2,3], Weiguang Wang[2,3*], Jie Chen[1*], Chong-Yu Xu[4], Hisashi Sato[5], Guoqing Wang[6]

[1]State Key Laboratory of Water Resources and Hydropower Engineering Science, Wuhan University, Wuhan, 430072, Peoples R China

[2]State Key Laboratory of Hydrology-Water Resources and Hydraulic Engineering, Hohai University, Nanjing, 210098, Peoples R China

[3]College of Hydrology and Water Resources, Hohai University, Nanjing, 210098, Peoples R China

[4]Department of Geosciences, University of Oslo, Oslo, N-0316, Norway

[5]Japan Agency for Marine-Earth Science and Technology, Yokohama, 236-0001, Japan

[6]Nanjing Hydraulic Research Institute, Nanjing, 210029, Peoples R China

[*]Ccorrespondence to: Weiguang Wang (wangweiguang2016@126.com); Jie Chen (jiechen@whu.edu.cn)

Abstract

Documenting year-to-year variations in carbon storage potential in terrestrial ecosystems is crucial for the determination of carbon dioxide (CO_2) emissions. However, the magnitude, pattern and inner biomass partitioning of carbon storage potential, and the effect of the changes in climate and CO_2 on inner carbon stocks, remain poorly quantified. Herein, we use a spatially explicit individual based-dynamic global vegetation model to investigate the influences of the changes in climate and CO_2 on the enhanced carbon storage potential of vegetation. The modelling included a series of factorial simulations using the CRU dataset from 1916 to 2015. The results show that CO_2 predominantly leads to a persistent and widespread increase in light-gathering vegetation biomass carbon stocks (LVBC) and water-gathering vegetation biomass carbon stocks (WVBC). Climate change appears to play a secondary role in carbon storage potential. Importantly, with the intensification of water stress, the magnitude of the light- and water-gathering responses in vegetation carbon stocks gradually decreases. Plants adjust carbon allocation to decrease the ratio between LVBC and WVBC for capturing more water. Changes in the pattern of vegetation carbon storage was linked to zonal limitations in water, which directly weakens and indirectly regulates the response of potential vegetation carbon stocks to a changing environment. Our findings differ from previous modelling evaluations of vegetation that ignored inner carbon dynamics and

32 demonstrates that the long-term trend in increased vegetation biomass carbon stocks is driven by CO_2

33 fertilization and temperature effects that are controlled by water limitations.

34 **1 Introduction**

35 As a result of the changes in climate and atmospheric carbon dioxide (CO_2), the terrestrial ecosystem

36 carbon cycle exhibits remarkable trends in interannual variations, which induce uncertainty in estimated

37 carbon budgets (Erb et al., 2018; Keenan et al., 2017). Recent studies assessing interannual fluctuations

38 in terrestrial carbon sinks have shown that the land carbon cycle is the most uncertain component of the

39 global carbon budget (Ahlstrom et al., 2015; Piao et al., 2020; Jung et al., 2017; Humphrey et al., 2018;

40 Gentine et al., 2019; Humphrey et al., 2021). These uncertainties result from an incomplete understanding

41 of vegetation biomass carbon production, allocation, storage, loss, and turnover time (Bloom et al., 2016).

42 The extent and distribution of vegetation carbon storage is central to our understanding of how to

43 maintain a balanced land carbon cycle. Changes in terrestrial vegetation carbon storage have a significant

44 effect on atmospheric CO_2 concentrations and determine whether biomes become a source or sink of

45 carbon (Erb et al., 2018; Humphrey et al., 2018; Terrer et al., 2021). Therefore, investigating the

46 processes producing changes in carbon storage is key to improving the accuracy of estimated terrestrial

47 carbon budgets, and to tap the greenhouse-gas moderation potentials of vegetation (Ipcc, 2007; Roy et

48 al., 2001).

49

50 The atmospheric CO_2 concentration is affected by the vegetation carbon stock, while the long-term trend

51 of vegetation carbon storage capacity is also affected by the changes in climate and CO_2. Since the

52 beginning of industrialization, there has been a noticeable enhancement in the plant capacity of storing

53 and sequestering carbon, which is needed for stabilizing greenhouse gas concentrations and mitigating

54 global warming (Chen et al., 2019; Pan et al., 2011; Le Noë et al., 2020; Magerl et al., 2019; Bayer et al.,

55 2015; Harper et al., 2018). Due to the interaction between terrestrial vegetation and a changing

56 environment, both photosynthesis and respiration of the vegetation also changed. To better absorb CO_2

57 and sunlight required for photosynthesis, vegetated zones are gradually covered by vegetation with

58 higher plant height and wider leaf area (Erb et al., 2008). This change has coincided with a widespread

59 change in other vegetation features, including a positive increase in annual gross primary productivity

and a greening of the biosphere (Madani et al., 2020; Zhu et al., 2016). The spatiotemporal distribution and environmental drivers in total carbon storage potential have been well documented on the basis of model estimates and satellite-based assessments (Erb et al., 2007; Erb et al., 2018; Bazilevich et al., 1971; Saugier et al., 2001; Bartholome and Belward, 2005; Olson et al., 1983; Pan et al., 2013; Ajtay et al., 1979; Ruesch and Gibbs, 2008; Kaplan et al., 2011; Shevliakova et al., 2009; Prentice et al., 2011; West et al., 2010; Hurtt et al., 2011). In contrast, the variability of inner components of carbon storage potential has not been extensively studied. Without an accurate assessment of the dynamics of each fraction, attribution of carbon storage potential to environmental drivers is highly uncertain. Consequently, partitioning potential vegetation carbon storage and revealing its inner processes are essential to accurately comprehend the current state of carbon storage capacity and reveal the influence of various drivers on the long-term trend of carbon storage potential.

The change of carbon storages in vegetation inner components is not only affected by environmental factors, but also controlled by allocation scheme of assimilated carbon. Fractional dynamics of the carbon stock are widely used as a key indicator to investigate the responses of vegetation to environmental drivers, which also reflect the response strategies of vegetation in environments with different water limitations (Yang et al., 2010). In arid regions, vegetation utilizes a tolerance strategy to allocate biomass, storing more biomass carbon in roots to resist enhanced water stress (Chen et al., 2013). Conforming to the optimal partitioning hypothesis, plants store more carbon in shoots and leaves in environments where water is more available and shift more carbon to roots when water is more limited (Yang et al., 2010; Mcconnaughay and Coleman, 1999). Water availability controls both carbon allocation and storage and can potentially transform zones characterized by a positive response to changes in climate and CO_2 to zones exhibiting a negative response. For example, global warming positively stimulates plant productivity (Keenan et al. 2017), while Madani et al. (2020) found that ~~plants productively with water stress show a negative response to temperature rise in tropical zones~~ productively showed a negative response to temperature in tropical zones due to increasing water stress. With increased warming, water limitations are predicted to increasingly reduce the proportion of leaves' biomass, and decrease plant photosynthesis (Ma et al., 2021). Water limitations have a strong regulating effect on the spatial pattern of change in vegetation carbon storage, demonstrating the effects of the changes in climate and CO_2 on

89 the dynamics of the plant organs are affected by the terrestrial water gradient. Thus, it is important to

90 systematically investigate the distinct responses of carbon storage potential to changes in climate and

91 CO_2 under differing conditions of water stress.

92

93 As documented above, many studies have investigated the total changes in zonal and global terrestrial

94 storage of carbon, while few studies have examined trends in the components partitioning of vegetation

95 carbon storage. Large gaps in our knowledge of the effects of various drivers on the partitioning of carbon

96 stocks in vegetation biomass remain. Meanwhile, plants adjust carbon allocation scheme to adapt to

97 environmental change. With increased warming, an increase in the magnitude of water stress may

98 dramatically change or even reverse the impact of these drivers on inner components of carbon storage

99 (Ma et al., 2021). Evaluating the response pattern of carbon stocks to various drivers under conditions of

100 limited water is elemental for clearly documenting the response mechanism of vegetation carbon storage

101 potential.

102

103 Here, we use a spatially explicit individual-based dynamic global vegetation model (SEIB-DGVM),

104 along with the components partitioning method to (1) systematically determine the long-term variability

105 of carbon storage potential and understand its response mechanisms, and (2) estimate trends in

106 partitioning of potential biomass carbon stocks of vegetation biomass. Throughout this study, the

107 potential biomass carbon stock, biomass carbon stored in vegetation without anthropogenic disturbance,

108 is recognized as an indicator of the potential of carbon storage by natural vegetation. Using a set of

109 factorial simulations to isolate responses to environmental change, we analyse the contributions of

110 multiple driving factors to the trends of two fractions of carbon stock at large scales individually. We

111 then conceptualize the role of water availability through an aridity index (AI), in which hydrological

112 zones are subdivided by their degree of aridity. By comparing the differences in the magnitude of

113 response between the fractions of light- and water-gathering carbon stocks for varying degrees of water

114 availability, we assess the effect of water limitations on the response pattern of potential carbon stocks

115 to changes in climate and CO_2.

2 Model description, experimental design, observational data, and evaluation metrics

In this section, we provided a list of data source (Sect. 2.1), an overview of the modelling concept (Sect. 2.2), the representation of biomass carbon stock partitioning in the SEIB-DGVM (Sect. 2.3), an overview of the experimental scheme used in the model simulations (Sect. 2.4), and an overview about data source and pre-processing of observation dataset for model evaluation (Sect. 2.5).

2.1 Forcing Data

Long-term daily meteorological time-series data are required to run model simulations, including precipitation, daily range of air temperature, mean daily air temperature, downward shortwave radiation at midday, downward longwave radiation at midday, wind velocity, and relative humidity. These data were obtained from the Climatic Research Unit (CRU) time series 4.00 gridded dataset (degree 0.5°) for the period 1901–2015 (Harris et al., 2020). Because the CRU dataset is a monthly based dataset, the monthly meteorological data were converted into daily climatic variables by supplementing daily climatic variability within each month using the National Centre for Environmental Prediction (NCEP) daily climate dataset. The NCEP data, displayed using the T62 Gaussian grid with 192 × 94 points, was interpolated into a 0.5° grid (which corresponds to the CRU dataset) using a linearly interpolation method. By combining the CRU data, with the interpolated NCEP dataset, we were able to directly obtain the most of driving meteorological data (details in Sato et al. (2020)). Neither the CRU nor NCEP datasets included downward shortwave and longwave radiation at midday. Thus, daily cloudiness values in the NCEP were used to calculate radiation values using empirical functions (Sato et al., 2007). These data were all aggregated to a daily timescale with 0.5° resolution to run SEIB-DGVM.

Atmospheric CO_2 concentrations were collected from Sato et al. (2020), which contains reconstructed CO_2 concentrations between 1901 and 2015. The statistical reconstruction of global atmospheric CO_2 was used in this analysis. These reconstructions were based on present annual CO_2 concentrations recorded from the Mauna Loa monitoring station. These data assume atmospheric CO_2 concentration was 284 ppm in 1750, and statistically interpolates atmospheric CO_2 concentrations to fill the gap from 1750 to 2015.

144   The physical parameters of the soil used in the model include soil moisture at the saturation point, field

145   capacity, matrix potential, wilting point and albedo. These data were obtained from the Global Soil

146   Wetness Project 2.

147   **2.2 Overview of modelling concept in SEIB-DGVM**

148   Model SEIB-DGVM version 3.02 (Sato et al., 2020) was employed in this study. This is a process-based

149   dynamic global vegetation model driven by meteorological and soil data. It is an explicit and

150   computationally efficient carbon cycle model designed to simulate transient effects of environmental

151   change on terrestrial ecosystems and land-atmosphere interactions. It describes three groups of processes:

152   land-based physical processes (e.g., hydrology, radiation, aridity), plant physiological processes (e.g.,

153   photosynthesis, respiration, litter), and plant dynamic processes (e.g., establishment, growth, mortality).

154   Twelve plant functional types (PFTs) were classified. During the simulation, a sample plot was

155   established at each grid ~~box~~cell, and then the growth, competition, and mortality of each the individual

156   PFTs within each plot were modelled by considering the specify conditions for that individual as it relates

157   to other individuals that surround it (Sato et al., 2007).

158

159   SEIB-DGVM treats the relationships between soil, atmosphere, and terrestrial biomes in a consistent

160   manner, including the fluxes of energy, water, and carbon. Based on specified climatic conditions and

161   soil properties, SEIB-DGVM simulates the carbon cycle, energy balance, and hydrological processes.

162   SEIB-DGVM utilizes three computational time steps: (1) During the growth phase, the metabolic

163   procedures including photosynthesis, respiration, and carbon allocation are executed for each individual

164   tree every simulation day. (2) The monthly process of tree growth including reproduction, trunk growth,

165   and expansion of a cross-sectional area of the crown are executed. (3) On the last day of each year, the

166   height of the lowest branch increases as a result of purging crown disks, or ~~self pruning~~self-pruning of

167   branches, at the bottom of the crown layer. The simulated unit of the model is a 30 m $\times$ 30 m spatially

168   explicit 'virtual forest'. A grass layer was placed under the woody layer, and provides for a

169   comprehensive, spatially explicit quantification of terrestrial carbon sinks and sources. The soil depth

170   was set at 2 m and was divided into 20 layers, each with a thickness of 0.1 m. The photosynthetic rate of

171   a single-leaf was simulated following a Michaelis-type function (Ryan, 1991). Respiration was divided

172   into two types: growth respiration and maintenance respiration. Growth respiration is defined as a

173   construction cost for plant biosynthesis, which is quantified by the chemical composition of each organ

174   (Poorter, 1994). Maintenance respiration of live plants occurs every day regardless of the phenological

175   phase, and is controlled by the temperature and nitrate content of each organ (Ryan, 1991). For a wide

176   variety of plant organs, the maintenance respiration rate is linearly related to the nitrogen content of

177   living tissue. The relative proportions of nitrogen in each organ for any PFT are linearly correlated. N-

178   deposition isn't included in SEIB-DGVM. Atmospheric CO_2 was envisioned to be absorbed by

179   photosynthesis of woody PFTs and grass PFTs. This assimilated carbon flux was then allocated into all

180   the plant organs (leaf, trunk, root, and stock), where maintenance respiration and growth respiration occur.

181   The hydrology module treats precipitation, canopy interception, transpiration, evaporation, meltwater,

182   and penetration.

183   **2.3 Carbon stock of vegetation biomass partitioning**

184   **2.3.1 Parameterization of daily allocation**

185   Flexible allocation schemes about resources and biomass are set up in the framework of the SEIB-DGVM

186   biogeochemical model. Based on the updated observation data, the allocation schemes of Boreal Needle-

187   leaved summer-green trees and Tropical Broad-leaved evergreen trees are improved at SEIB-DGVM

188   V3.02. Allocation schemes of other PFTs are the same as the original version. Atmospheric CO_2 is

189   assimilated by the photosynthesis of both woody and grass foliage, and then is added into the non-

190   structural carbon of the plant. This non-structural carbon of photosynthetic production is allocated to all

191   the plant organs (foliage, trunk, root, and stock), supplying what is needed for the maintenance and

192   growth of each organ. When the non-structural carbon is greater than 0 during the growth phase, the

193   following dynamic carbon allocation is executed for each individual plant at the daily time scale, such

194   that:

195   (1) When the fine root biomass ($mass_{root}$) of wood or grass does not satisfy minimum requirements for

196   fulfilling functional balance ($mass_{leaf}/FR_{ratio}$), the mass of non-structural carbon is allocated to the root

197   biomass to supplement the deficit. Here, $mass_{leaf}$ is the leaf biomass, and FR_{ratio} is the ratio of $mass_{leaf}$ to

198    $mass_{root}$ satisfying the functional balance.

199   (2) The stock biomass is supplemented until it is equal to leaf biomass. This scheme is active after the

200   first thirty days of the growing phase.

201   (3) Woody leaf biomass is constrained by three limitations of the maximum leaf biomass, which are

202   calculated as follows:

203   $$max_1 = \left(crown_{area} + \pi crown_{diameter} crown_{depth}\right)\frac{LA_{max}}{SLA} \tag{1}$$

204   $$max_2 = ALM_1 \frac{\pi\left(dbh_{heartwood}/2 + dbh_{sapwood}/2\right)^2 - \pi\left(dbg_{heartwood}/2\right)^2}{SLA} \tag{2}$$

205   $$max_3 = \frac{mass_{available}}{RG_f} \tag{3}$$

206   $$mass_{leaf} = \min(max_1, max_2, max_3) \tag{4}$$

207   where max_1, max_2, and max_3 are, respectively, maximum leaf biomass for a given crown surface

208   area, cross-sectional area of sapwood, and non-structural carbon; SLA is a constant of PFTs leaf area

209   (m^2 g^{-1}); LA_{max} is the plant functional type specific maximum leaf area per unit crown surface area

210   excluding the bottom layer (m^2 m^{-2}); ALM_1 represents the area of transport tissue per unit biomass, and

211   is a constant (dimensionless). If the mass$_{leaf}$ is less than the minimum (max_1, max_2, max_3), the mass of

212   non-structural carbon is allocated into leaf biomass to supplement the deficit.

213   When the leaf area index of grass equals the optimal leaf area index, it stops to allocate non-structural

214   carbon to grass leaf, which is calculated as:

215   $$lai_{opt} = \frac{\ln par_{grass} - \ln\left\{\frac{p_{sat}}{lue}\left[\left(1 - \frac{cost/SLA}{0.09093 \times dlen \times p_{sat}}\right)^{-2} - 1\right]\right\}}{eK} \tag{5}$$

216   where lai_{opt} is the optimal leaf area index (m^2 m^{-2}); par_{grass} is the grass photosynthetically active

217   radiation (μmol photon m^{-2} s^{-1}); p_{sat} is the light-saturated photosynthetic rate (μCO_2 m^{-2} s^{-1}); lue is

218   the light-use efficiency of photosynthesis (mol CO_2 mol photon^{-1}); $cost$ is the cost of maintaining

219   leaves per unit leaf mass per day (g DM g DM^{-1} day^{-1}); $dlen$ is day length (hour); and eK is light

220   attenuation coefficient at midday.

221   (4) When non-structural carbon is less than 10 g dry mass (DM) PFT^{-1} or annual NPP is less than 10 g

222   DM PFT^{-1} in the previous year, the following daily simulation processes (5-6) will be skipped.

223   (5) When total woody biomass is more than 10 kg DM, which defines the minimum tree size for

224   reproduction, 10% of non-structural carbon is used for every daily process of reproduction, including

225   having flowers, pollen, nectar, fruits, and seeds. These organs are not explicitly modelled in SEIB-

226   DGVM.

227   (6) During the simulation of trunk growth, the remaining non-structural carbon is allocated to sapwood

228   biomass. There is no direct allocation to heartwood, which is transformed slowly from sapwood biomass.

229   For grass PFTs biomass, the densities of all organs comprising the biomass never decline below 0.1 g

230   DM m^{-2} even if the environment is deteriorated for grass survival. A more detailed description of SEIB-

231   DGVM is given by Sato et al. (2007).

232

233   To control plant phenology and the rate of photosynthesis as a function of the limitation in terrestrial

234   water, the physiological status of the limitation of terrestrial water is calculated as:

235    $$p_{sat} = PMAX \, ce_{tmp} ce_{co_2} ce_{water} \tag{6}$$

236    $$ce_{water} = \sqrt{stat_{water}} \tag{7}$$

237    $$stat_{water} = \frac{max(pool_{w(1)}/Depth_{(1)}, \; pool_{w(2)}/Depth_{(2)}) - W_{wilt}}{W_{fi} - W_{wilt}} \tag{8}$$

238   where p_{sat} is the single-leaf photosynthetic rate of tree PFTs and grass PFTs (μmol CO$_2$ m^{-2} s^{-1});

239    $PMAX$ is the potential maximum of photosynthetic rate (μmol mol^{-1} CO$_2$ m^{-2} s^{-1}); ce_{tmp} and ce_{co_2} are

240   the temperature and CO$_2$ concentration effect coefficient (dimensionless), separately; ce_{water} is the

241   water effect coefficient (dimensionless); $stat_{water}$ is the physiological status of the terrestrial water

242   limitation, which ranges between 0.0–1.0, dimensionless; $pool_{w(n)}$ is the water content in soil layer n,

243   mm; $Depth_{(n)}$ is the depth of the soil layer n, mm; W_{wilt} is soil moisture at the wilting point, m m^{-1};

244   and W_{fi} is soil moisture at field capacity, m m^{-1}. When the temperature of all soil layers is less than 0°

245   C, $stat_{water}$ is equal to 0.

246   **2.3.2 Carbon stock partitioning method**

247   SEIB-DGVM allocates and stores the biomass carbon in four pools of woody PFT (foliage, trunk, root,

248   and stock) and three pools of grass PFT (foliage, root, and stock). To investigate the fractional variability

249   of carbon sequestration potential between the pools, we partitioned potential vegetation carbon stocks

250   based on the physiological function of the plant (Figure A1). The root-shoot ratio (R/S) has been used to

251   distinguish and investigate the ratio of below-ground biomass (root biomass) and above-ground biomass

252   (shoot biomass) (Zhang et al., 2016). In this study, we adjusted the method of calculating the R/S ratio

253   by distinguishing between the light-gathering vegetation biomass carbon stock (LVBC) and the water-

254   gathering vegetation biomass carbon stock (WVBC). LVBC represents the biomass carbon invested by

255   plant is used to gather sunlight, including biomass carbon from woody foliage, woody trunk, and grass

256   foliage. WVBC represents biomass carbon used to gather water, including biomass carbon from woody

257 fine roots and grass fine roots, excluding the stock pool. Stock biomass is used for foliation after dormant

258 phase and after fires, which is reserve resource in each individual tree. Fine root biomass is just a tiny

259 fraction to the total biomass, but is has a very high turnover rate and determines the capacity of vegetation

260 to absorb soil water. Thus,

261 $$\frac{LVBC}{WVBC} = \frac{Tmass_{leaf} + Tmass_{trunk} + Gmass_{leaf}}{Tmass_{root} + Gmass_{root}} \times 100\% \tag{9}$$

262 where *LVBC* is light-gathering vegetation biomass carbon stock (kg C m^{-2}); *WVBC* is water-gathering

263 vegetation biomass carbon stock (kg C m^{-2}); $Tmass_{leaf}$ is the leaf biomass carbon stock of woody

264 vegetation (kg C m^{-2}); and $Tmass_{trunk}$ is the trunk biomass carbon stock of trees (kg C m^{-2}), including

265 both branch and structural roots. This biomass is simplistically attributed to light-gathering vegetation

266 organs and is used primarily to support the plant. $Gmass_{leaf}$ is the leaf biomass carbon stock of grass

267 (kg C m^{-2}); whereas $Tmass_{root}$ and $Gmass_{root}$ are functional root (fine roots) biomass carbon stocks

268 of trees and grass, separately (kg C m^{-2}), which absorb water and nutrition from soil.

269 **2.4 Experimental design**

270 **2.4.1 Setup of model runs**

271 SEIB-DGVM simulations begin with seeds of selected PFTs planted in bare ground. The establishment

272 of PFTs seeds are determined by the climatic conditions in each grid cell. We inputted the transient

273 climate data from 1901 to 1915 to spin up the model in a repetitive loop. No obvious trend in climatic

274 factors was observed during this period (Tei et al., 2017). A spin-up period of 1050 years was necessary

275 to bring the terrestrial vegetation carbon cycle into a dynamic equilibrium. To reach quasi-equilibrium

276 in the vegetation biomass, about 1000 years of simulation was required as a spin-up procedure.

277 **2.4.2 Factorial simulation scheme**

Table 1. List of factorial simulations used in this study

Factorial simulation	CO$_2$ concentration	Precipitation	Temperature	Radiation	Other drivers
S1	√	√	√	√	√
S2	√				
S3	√	√			
S4	√		√		
S5	√			√	
S6	√				√

10

278 In order to further quantify the relative contributions of varying atmospheric CO_2 concentrations,

279 precipitation, temperature, radiation, and other factors (wind velocity and relative humidity), we

280 performed six factorial simulations. In simulation S1, atmospheric CO_2 concentration and all of climate

281 variables were varied. In simulation S2, only atmospheric CO_2 concentration was varied, and climate

282 variables were held constant (Climate variables of the transient period (1901-1915) were repeatedly

283 inputted). In simulation S3 (or S4, S5), atmospheric CO_2 and precipitation (or temperature, radiation)

284 were varied, and other climate variables were held constant. In simulation S6, atmospheric CO_2, wind

285 velocity, and relative humidity were varied, and other climate variables were held constant. Finally, S2

286 was used to evaluate the effects of CO_2 fertilization on carbon stock variation. The differences of S2-S3,

287 S2-S4, S2-S5, and S2-S6 were used to evaluate the response of carbon stock growth to precipitation,

288 temperature, radiation, and other drivers, respectively.

289 **2.4.3 Non-parametric test methods**

290 Each driving factor (atmosphere CO_2, precipitation, temperature, and radiation) has a different influence

291 on the carbon stock, so it is difficult to make a simple pre-assumption about the population distribution

292 pattern for factorial simulations. We used the non-parametric Mann-Kendall and Sen's slope estimator

293 statistical tests (Gocic and Trajkovic, 2013) to assess the ability of SEIB-DGVM to simulate the response

294 patterns of carbon storage potential to a change in climate and CO_2 concentrations. We regressed the

295 simulated hundred-year mean global average carbon stock time series to reveal the accumulative

296 influences of the single variables based on the factorial simulations where only one or two drivers were

297 varied. As shown in Figures A2 and A3, detection trends of LVBC and WVBC for all driving factors

298 performed statistically well (in agreement at the 95% confidence intervals), indicating this analytical

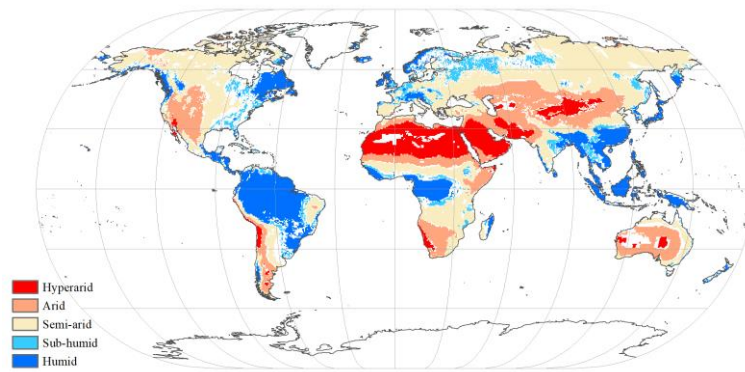299 method was suitable for trend attribution at the global scale.

2.4.4 Distinguishing hydrological regions

Figure 1. Global spatial patterns of water availability. Spatial variations in water availability were categorized based on the multiyear average aridity index (AI), defined as the ratio of the multiyear mean precipitation to the potential evapotranspiration. Categories include: hyper-arid (AI ≤ 0.05), arid (0.05 < AI ≤ 0.2), semi-arid (0.2 < AI ≤ 0.5), sub-humid (0.5 < AI ≤ 0.65), and humid (AI > 0.65). The white grid cell was not assigned hydrological category.

301 Locally available water strongly regulates and limits the response of carbon stocks to changes in climate

302 and CO_2. We used aridity index (AI) to distinguish between the global hydrological regions for

303 comparing the long-term trend in carbon stocks over different hydrological environments, and for

304 quantifying the influences of each hydrological environment on the variations in the trends. The AI was

305 defined as:

306 $$AI = \frac{\bar{P}}{\overline{ET_p}} \tag{10}$$

307 where $\bar{P}$ is the multiyear mean precipitation (mm year^{-1}); and $\overline{ET_p}$ is the multiyear mean potential

308 evapotranspiration (mm year^{-1}), which was calculated by the Penman-Monteith model (Monteith and

309 Unsworth, 1990). As in a previous study (Chen et al., 2019), five hydrological regions were categorized

310 based on AI value. Under the influences of climate change, the hydrological condition was changed in

311 some grid cells (Figure A4). For example, the grid cell classified as sub-humid zone in the period of

312 1916-1945 was redefined as semi-arid zone in the period of 1986-2015. In this study, gird cells with

313 consistent hydrological condition between the period of 1916-1945 and the period of 1986-2015 were

314 selected and classified (Figure 1).

2.5 Observation dataset for model evaluation

A global time series of potential vegetation carbon was modelled by the SEIB-DGVM between 1916-2015. In terrestrial vegetation biomes, there is a high correlation between biomass carbon stock density and NPP per unit (Erb et al., 2016; Kindermann et al., 2008) (Figure A1). Thus, we collected NPP observation dataset and used NPP as a proxy of the carbon stock to assess model accuracy. Ecosystem Model-Data Intercomparison (EMDI) builds upon the accomplishments of the original worldwide synthesis of NPP measurements and associated model driver data prepared by Global Primary Production Data Initiative. We obtained the monitoring station data from the EMDI working group, and then compared their data with modelled multiyear average NPP in the period of 1916-1999 (Figure 2).

Multiyear average NPP simulated by SEIB-DGVM (gC m^{-2} yr^{-1})
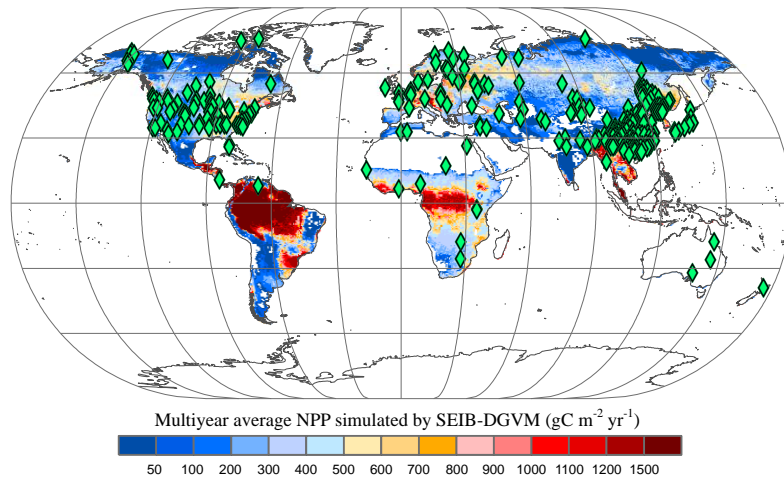
Figure 2. Multiyear average NPP simulated by SEIB-DGVM and EMDI global site distribution.
Green rhombuses indicate the monitoring stations of the EMDI.

However, *in-situ* observations are sparse for global spatial-temporal validation. Therefore, we used the MOD17A3 products to further verify the simulated potential NPP in the twenty first century. These data were collected by the Moderate Resolution Imaging Spectroradiometer and are some of the most widely used data to assess the accuracy of global model simulations (Gulbeyaz et al., 2018). The natural vegetation zones refer to the hypothetical condition that would prevail in an assumed absence of anthropogenic activity, but under historical climate fields (Erb et al., 2018; Haberl et al., 2014). The potential NPP is defined as that assimilated carbon stored in natural vegetation without the disturbance of anthropogenic activities (Erb et al., 2018).

In order to distinguish the distribution of vegetation ~~zones~~ gird cells without anthropogenic disturbance,

we obtained global land cover types in the period 2001-2015 from MCD12C1 (Table A1). We included grid cells whose largest vegetation component ~~defined vegetation grid cells as those whose largest component~~ was evergreen needleleaf forest, evergreen broadleaf forest, deciduous needleleaf forest, deciduous broadleaf forest, mixed forest, closed shrublands, open shrublands, woody savannas, savannas or grasslands. Other grid cells were excluded from our analysis.

Part of grid cells covered by grassland were grazed by livestock, leading to the decrease of NPP of grass PFTs. There is a weak anthropogenic disturbance in rangeland, while managed pasture is intensely grazed by livestock. To remove pasture area with strong anthropogenic disturbance, ~~We~~ we obtained land-use forcing data from Land-Use Harmonization (LUH2) to map the distribution of managed pasture data from 2001 to 2015 (Hurtt et al., 2020). As shown in Figure A5, grassland in eastern Asia, western Europe, south central Africa, and western South America were severely affected by grazing. For exhibit the disturbance of managed pasture, we calculated the mean fraction of managed pasture within the corresponding 0.5° grid unit. When the fraction of managed pasture over 10%, the grid cell was considered to be affected by managed pasture. To reduce the interference effects of livestock grazing, we first removed the grid cells ~~–~~ affected by managed pasture. Then, we map the distribution of natural vegetation ~~zones~~ grid cells without anthropogenic disturbance (Figure A6). ~~We declare that t~~This exclusion method is only used for potential NPP comparison.

3 Results and discussion

3.1 Evaluation of SEIB-DGVM

Figure 3 illustrates the comparison between model simulated and observed multi-year mean NPP during 1916-1999. The determined coefficient (R^2) between EMDI observed and estimated multiyear average NPP of 669 *in-situ* observations is 0.54, which is significant at the p=0.01 level. The slope of the regressed line is 0.70 during the twentieth century.
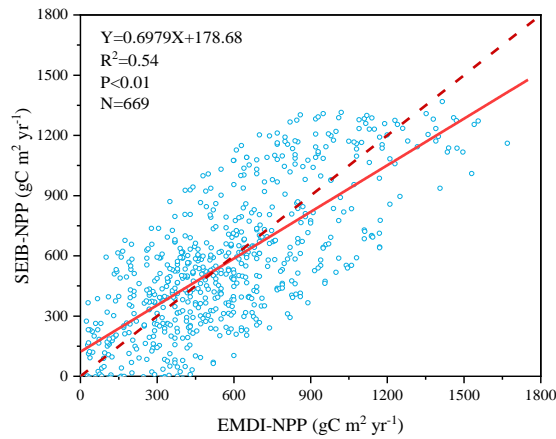
Figure 3. Comparison of multiyear average NPP calculated by SEIB-DGVM and EMDI for the twentieth century. The solid line is the best fit curve; and the dashed line represents a perfect correspondence in the results of the two.

358 Based on land cover types dataset from 2001 to 2015, we obtained NPP-MOD17A3 data in natural

359 vegetation zones without anthropogenic disturbance at the same period. Figure 4 shows that the modelled

360 NPP from the SEIB-DGVM exhibited a high degree of consistency with the NPP-MOD17A3 data in

361 natural vegetation zones over the period (R^2=0.63, p<0.05). The general spatiotemporal agreement

362 between the simulated NPP derived from SEIB-DGVM with *in-situ* observations and derived from

363 satellites reveals that it is reasonable to use the SEIB-DGVM simulations to evaluate the same

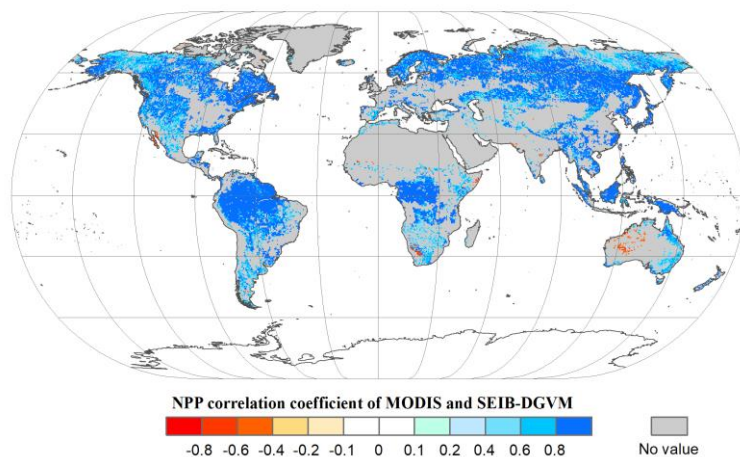364 mechanisms controlling global potential biomass carbon stocks of vegetation.

Figure 4. Spatial patterns in the potential NPP correlation coefficients (P<0.05) between SEIB-DGVM and MODIS between 2001–2015. These data were used to validate SEIB-DGVM.

365 Finally, the modelled result of potential vegetation biomass carbon stock was compared with current

366 existing data from the literature and state-of-the-art datasets. Figure 5 shows that the modelled results are

367 within the range of potential carbon stocks, which indicate that the SEIB-DGVM reliably simulated the
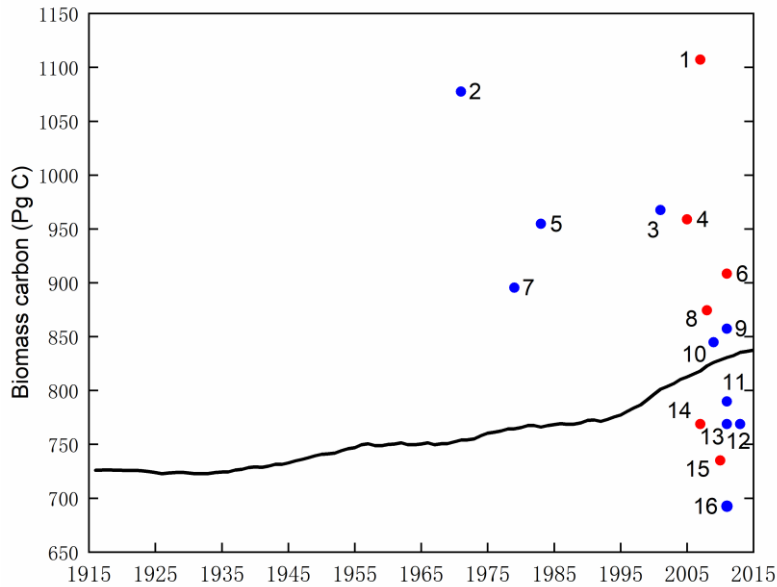
368 carbon stock dynamics.

Figure 5. Estimates of the potential vegetation biomass carbon stock from the literature (blue plot), state-of-the-art datasets (red plot) and this study (black line). Datasets are from the following studies: (1)(Erb et al., 2018; Erb et al., 2007), (2)(Bazilevich et al., 1971), (3)(Saugier et al., 2001), (4)(Erb et al., 2018; Bartholome and Belward, 2005), (5)(Olson et al., 1983), (6)(Erb et al., 2018; Pan et al., 2011), (7)(Ajtay et al., 1979), (8)Erb et al., 2018; Ruesch and Gibbs, 2008), (9)(Kaplan et al., 2011), (10)(Shevliakova et al., 2009), (11)(Kaplan et al., 2011), (12)(Pan et al., 2013), (13)(Prentice et al., 2011), (14)(Erb et al., 2018; Erb et al., 2007), (15)(Erb et al., 2018; West et al., 2010), (16)(Hurtt et al., 2011).

369 **3.2 Enhanced carbon stocks and its fractions**

370 We distinguished the changes of LVBC and WVBC from total vegetation carbon stocks. The historical

371 temporal trends over the period are ~~showed~~ shown in Figure 6a. The potential vegetation carbon stock

372 exhibits a net increase of 119.26 ± 2.44 Pg C in the last century (± 2.44 represents intra-annual fluctuation

373 in carbon stock, which is the difference between maximum value and minimum value of carbon stock

374 within the year). Based on Pearson correlation analysis, this increasing trend of annual average carbon

375 stock exhibits a robust agreement with the dramatic increase in atmospheric CO_2 concentration

376 ($R^2=0.9677$, $p<0.001$), suggesting that the carbon stock is strongly affected by CO_2 fertilization.

16

377 Meanwhile, the positive correlation between the carbon stock and CO_2 generally extends across LVBC

378 (R^2=0.9669) and WVBC (R^2=0.9622). After the value of the global terrestrial carbon stock and trends

379 were partitioned among the vegetation functional classes, we see that LVBC increases 116.18 ± 2.34 Pg

380 C (or ~15.60%), which explains 97.42% of total carbon stock increasing trend and dominates the positive

381 global carbon stock trend; WVBC also increases 3.08 ± 0.14 Pg C (or ~18.03%) over the past century.
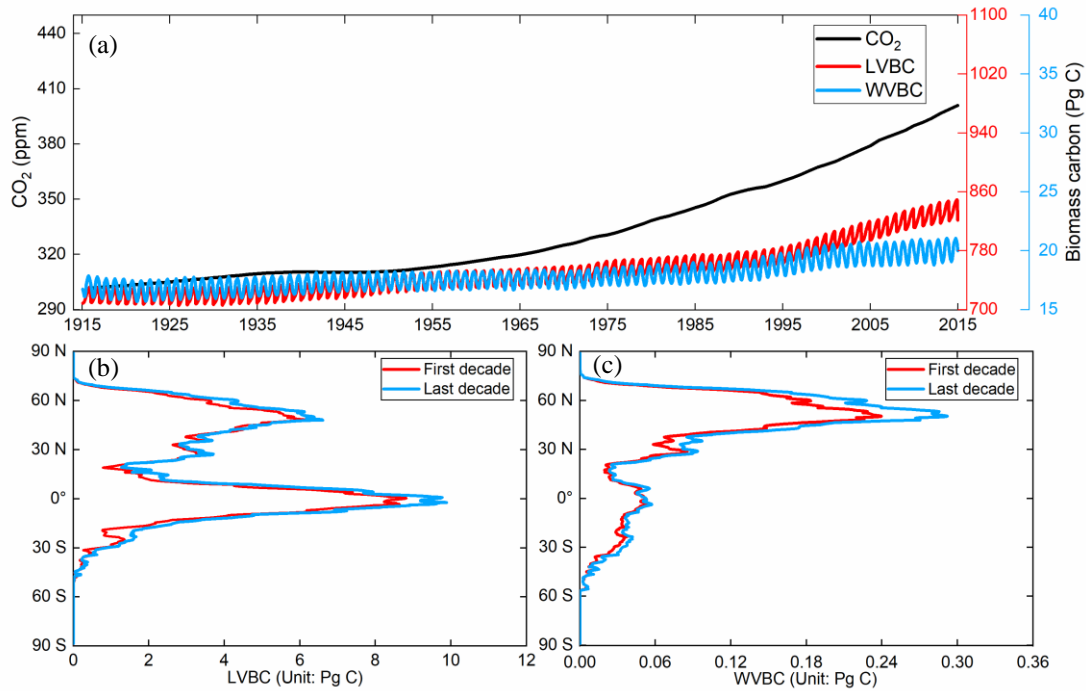
Figure 6. Global potential biomass carbon stocks of vegetation during the past 100 years. (a) The

evolution of global potential biomass stocks (LVBC+WVBC), along with changes in biomass stocks

that can be attributed to the variability and trend of LVBC and WVBC through the twentieth century.

The red line represents the monthly value of LVBC, the blue line represents the monthly value of

WVBC, and the black line represents the annual value of CO_2 concentration. (b, c) Zonal averaged

sums of the annual LVBC and WVBC for latitudinal bands during the first decade (1916–1925, red

line) and the last decade (2006–2015, blue line) shows the increased carbon stock capacity.

382 The global distributions of the decadal-average change in LVBC and WVBC are shown in Figures 6b

383 and 6c, respectively. The significant historical changes in climate and CO_2 enhance the carbon stock of

384 the terrestrial ecosystem, and their positive influences are broadly distributed across a latitudinal north–

385 south gradient. The latitudinal bands of increasing annual LVBC are mainly distributed in the tropical

386 and boreal latitudes, which is consistent with Figure 7b. The decadal and inter-annual variabilities of

387 LVBC are dominated by the tropical and ~~semi-arid~~boreal zones where large portions of the zones are

388 highly productive (Ahlstrom et al., 2015; Poulter et al., 2014). Tropical LVBC dominates the long-term

389 trend of global LVBC in the last hundred years. Compared with LVBC, the increase of tropical WVBC

390 is light. There is a single peak in the spatial variation of annual WVBC (Figure 6c and Figure 7c). WVBC

391 exhibits robust growth at most latitudes, and increases mainly in boreal latitudes.

392 **3.3 Spatial variability in estimated LVBC and WVBC trends**

393 In Figures 7(a) and 7(b), total carbon stock and LVBC exhibited a significantly increasing trend in eastern

394 South America, southern Africa, and northern Asia, while they declined in central North America,

395 northwest South America, and central Africa. WVBC showed a more widely increasing tendency in

396 North America, southeastern South America, and Europe, while had a decreasing trend in part zones of

397 Asian. We find that the total carbon stock as well as the light- and water-gathering vegetation biomass

398 carbon stocks over the period of 1916–2015 exhibited a remarkable spatial heterogeneity. Figure 7a

399 shows that an increase in vegetation carbon stocks occurred over zones and global aggregate levels during

400 the entire study period. About 57.39% of the terrestrial grid cells exhibited an increase with a noticeable

401 trend (p<0.05) in biomass carbon stock; 53.82% of global grid cells possessed increases that were

402 statistically significant at the p=0.01 level. To determine the contributions of each fraction (LVBC,

403 WVBC) to the total change in the potential vegetation carbon stock, we partitioned and present the

404 historical spatial and temporal patterns for each fraction separately (Figure 7b, 7c). LVBC contributes

405 97.33% to the incremental change of total carbon stock (116.18 ± 2.34 Pg C), with about 51.32% of the

406 grid cells possessing a noticeable positive trend (p=0.01). Generally, spatial patterns of LVBC and the

407 total carbon stock are consistent (Figure 7a, 7b), which further supports the argument that LVBC

408 dominates the trend in carbon stocks in most zones. Although the proportion of the total change in carbon

409 stocks is small (2.58% of total carbon stock increase), about 61.00% of the land surface shows an increase

410 in WVBC; of these terrestrial grid cells, 55.81% was characterized by a significant p=0.01 increase.
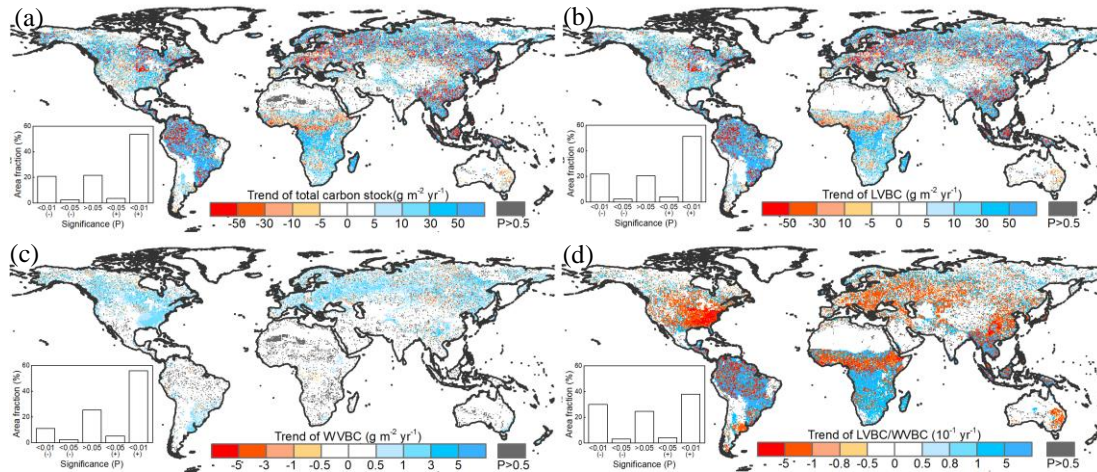
18

Figure 7. Spatial patterns in the trends of potential vegetation carbon stocks and their fractions from 1916 to 2015. Difference induced by changes in climate and CO_2 in terrestrial biomass carbon stock (a), LVBC (b), and WVBC (c) during the historic period 1916–2015. The blue bar indicates the significantly increasing trends and the red bar indicates the significantly decreasing trends in carbon stocks. (d) Trend in the LVBC/WVBC ratio from 1916 to 2015. The blue bar indicates significantly increasing trends in the ratio, and vice versa. The grey bar indicates the trend is statistically insignificant (P >0.05). The sub-graphs show the significant test results. A '+' symbol indicates a positive trend, and vice versa.

411   Under the influences of a changing climate and CO_2 concentrations, there is a slight increase in the ratio

412   of global LVBC/WVBC; the rate of increase is 0.0171 yr^{-1} in the last hundred years, which is significant

413   at the 0.01 level (Figure 7d). About 42.08% of the terrestrial grid cells exhibits an increase with a

414   noticeable trend (p<0.05) in the ratio of LVBC and WVBC; 37.95% of global grid cells possessed

415   increases that are statistically significant at the p=0.01 level. Meanwhile, 33.32% of the land surface

416   shows a significant decrease in LVBC/WVBC; of these terrestrial grid cells, 30.06% is characterized by

417   a significant p=0.01 decrease. ~~Zones~~ Gird cells with noticeable increases in the ratio of LVBC to WVBC

418   are mainly located in southern Africa, central South America, and northern Eurasia. Negative trends in

419   LVBC/WVBC ratios are found in northern America, southern Europe, and tropical Africa.

420   **3.4 Responses of LVBC and WVBC to environmental drivers**

421   The responses of LVBC and WVBC to changes in climate and CO_2 are both positive at the global level

422   (Figure 8a, 8c), although zonally, they exhibit both negative and positive responses (Figure 8b, 8d).

423   Based on the results of factorial simulations and Mann-Kendall+Sen tests, CO_2 fertilization explains the

largest proportion of the change in the carbon stock; about 82.45% change in LVBC was positive (Figure

8a), whereas 89.28% of the change in WVBC was positive (Figure 8c). In factorial simulation S2, the

long-term trend of LVBC was 15.521 g C m^{-2} yr^{-1} and that of WVBC was 0.435 g C m^{-2} yr^{-1} at the

period from 1916 to 2015 (Figure A2a and Figure A3a). The separately simulated LVBC and WVBC

increased by 80.98 Pg C and 2.66 Pg C with increasing atmospheric CO_2 concentrations (from 301.73

ppm in 1916 to 400.83 ppm in 2015). The other climatic drivers (precipitation, temperature, radiation,

humidity, and wind speed) remained at baseline values. While the increase or decrease in the carbon

stock may be attributed to more than one driving factor, within any specified grid cell, the one with the

highest positive or negative contribution is the ~~dominated~~ dominant driver that consistently resulted in

the highest increase or decrease in the carbon stock for that grid cell. The spatial pattern illustrates that

CO_2 dominates the variability in LVBC in 7.28% of the ~~zones~~grid cells, including 1.21% of the ~~zones~~

grid cells that exhibited a negative change and 6.07% that exhibited a positive change (Figure 8b). CO_2

dominates the variability in WVBC in 27.60% of the ~~zones~~grid cells, including 1.73% of the ~~zones~~ grid

cells that exhibited a negative change and 25.87% of ~~zones~~ grid cells with a positive change (Figure 8d).

Under the effect of CO_2 fertilization, grid cells with increased trend in WVBC mainly distribute in boreal

latitudes (Figure 6c). These trends are consistent with ~~and~~ previous studies (Tharammal et al., 2019; Zhu

et al., 2016; Keenan et al., 2017) in which positive trends occurred, especially for WVBC.
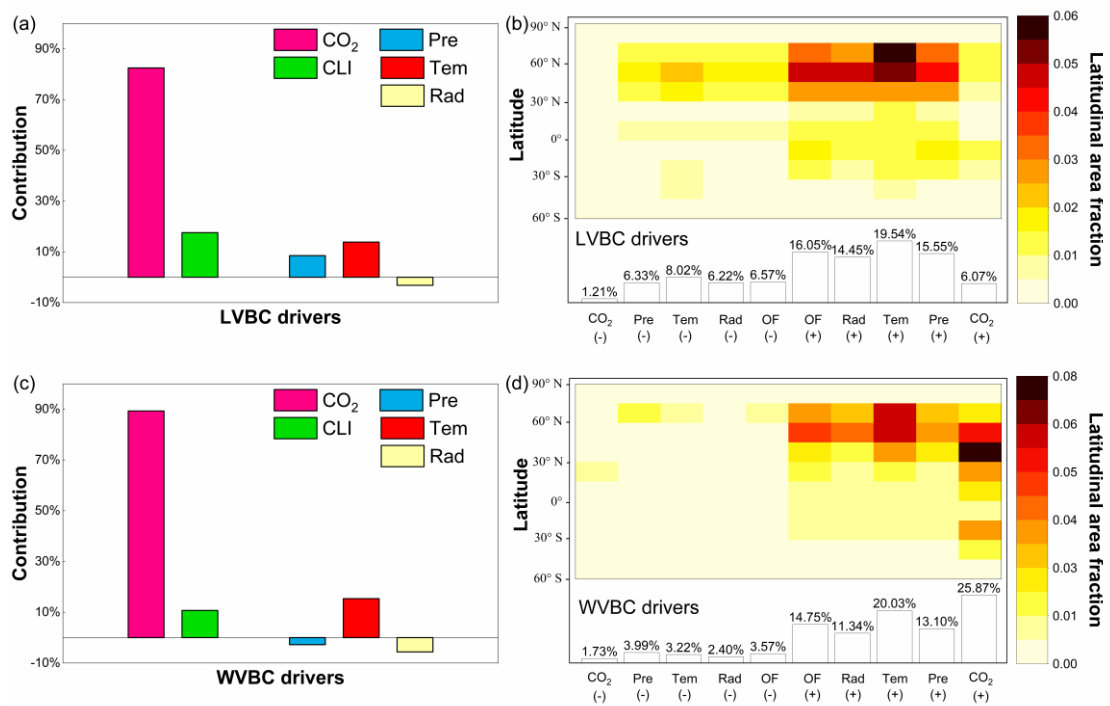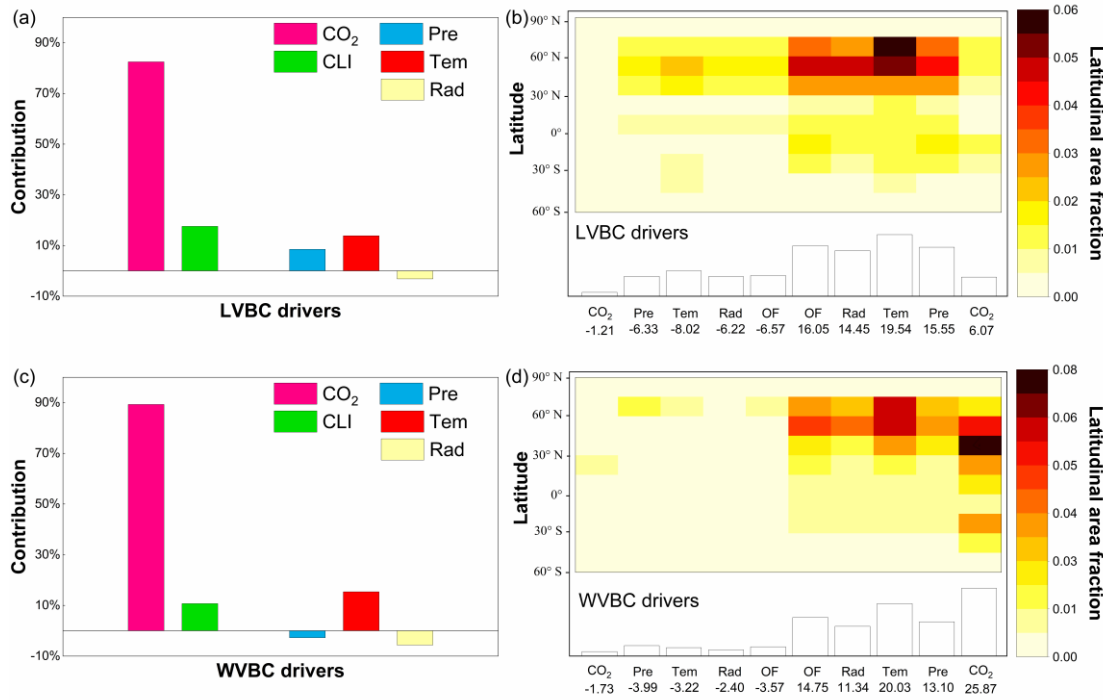
Figure 8. The proportion of changes in ~~the~~ vegetation biomass carbon stocks attributed to driving factors. Ratios of the driving factors of CO_2 fertilization effects (CO_2), climate change effects (CLI), precipitation (Pre), temperature (Tem), radiation (Rad) for LVBC (a) and WVBC (c) ~~under the five scenarios using~~are calculated by the Mann-Kendall and Sen's slope estimator statistical tests. Attribution of LVBC (b) and WVBC (d) dynamics to driving factors calculated as averages along 15° latitude bands. At the local scale~~s~~, the driving factors include CO_2, Pre, Tem, Rad, and other climate factors (OF). The fraction of global ~~area~~ grid cells (%) that is predominantly influenced by the driving factors is showed at the bottom of the bar. The '-' symbol before fraction indicates a negative effect of the driving factor on carbon stock, and vice versa.

441 Climate change induced by the greenhouse effect explains part of the increase in carbon stocks, but unlike

442 CO_2 fertilization, climate has dramatic negative effects on some vegetated zones. Figure 8a illustrates

443 that temperature is the largest climatic contributor to the change in LVBC (13.83%, 2.572 g m^{-2} yr^{-1}),

444 followed by precipitation (8.51%, 1.572 g m^{-2} yr^{-1}) and radiation (–3.19%, –0.649 g m^{-2} yr^{-1}). The spatial

445 distribution shows that temperature predominantly influences the change in LVBC (Figure 8b),

446 influencing over 27.56% of the global vegetated ~~zones~~grid cells, followed by precipitation (21.88%) and

447 radiation (20.67%). Figure 8c shows there are negative effects and contributions of precipitation on the

448 change in WVBC at the global level (–2.76%, –0.013 g m^{-2} yr^{-1}). Temperature is the largest climatic

21

449   contributor to the change in WVBC (15.36%, 0.075 g m^{-2} yr^{-1}), followed by radiation (-5.63%, -0.027 g

450   m^{-2} yr^{-1}). Modelled WVBC trends based on the factorial simulations have similar spatiotemporal patterns

451   to LVBC (Figures A2 and A3), and the spatial patterns of light- and water-gathering carbon stocks show

452   a significantly increasing trend in the most of boreal zones. In the Southern Hemisphere, the trends of

453   WVBC are extensively statistically insignificant in all factorial simulations, and only a small proportion

454   of grid cellss show a significantly increasing trend. There is a significantly increasing trend in LVBC in

455   south-central Africa and northern South America. The effects of temperature on WVBC are stronger than

456   LVBC, because temperature has a stronger effect on the metabolism process of root growth, dominating

457   the turnover rate and the costs of maintenance respiration in root growth process (Gill and Jackson, 2000).

458   It should be noted that trends in the global carbon stock can be largely attributed to the influences of CO_2,

459   precipitation, temperature, and radiation (Figure 8). Nonetheless, at the zonal scale, the contributions of

460   other factors should be considered, such as humidity and wind speed. The effects of these other factors

461   dominate trends in LVBC in over 16.05% of the zones grid cells that increased and 6.57% of the zones

462   grid cells that decreased. In the case of changes in WVBC, other factors were dominant drivers in over

463   14.75% of the zones grid cells that increased and 3.57% of zones grid cells that decreased. Under the

464   effect of climate, the variability of LVBC and WVBC is positive in most zonesgrid cells, promoting the

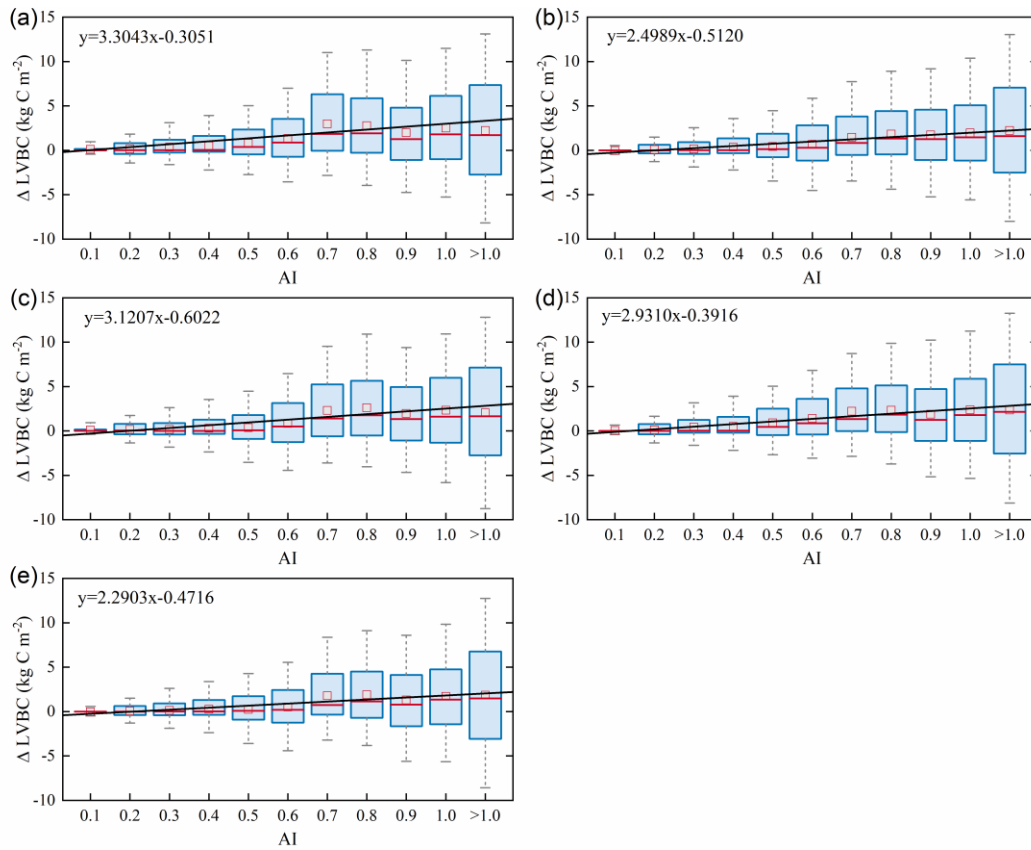465   noticeable increase of carbon stocks in boreal latitudes.

3.5 Constraints imposed by water limitations
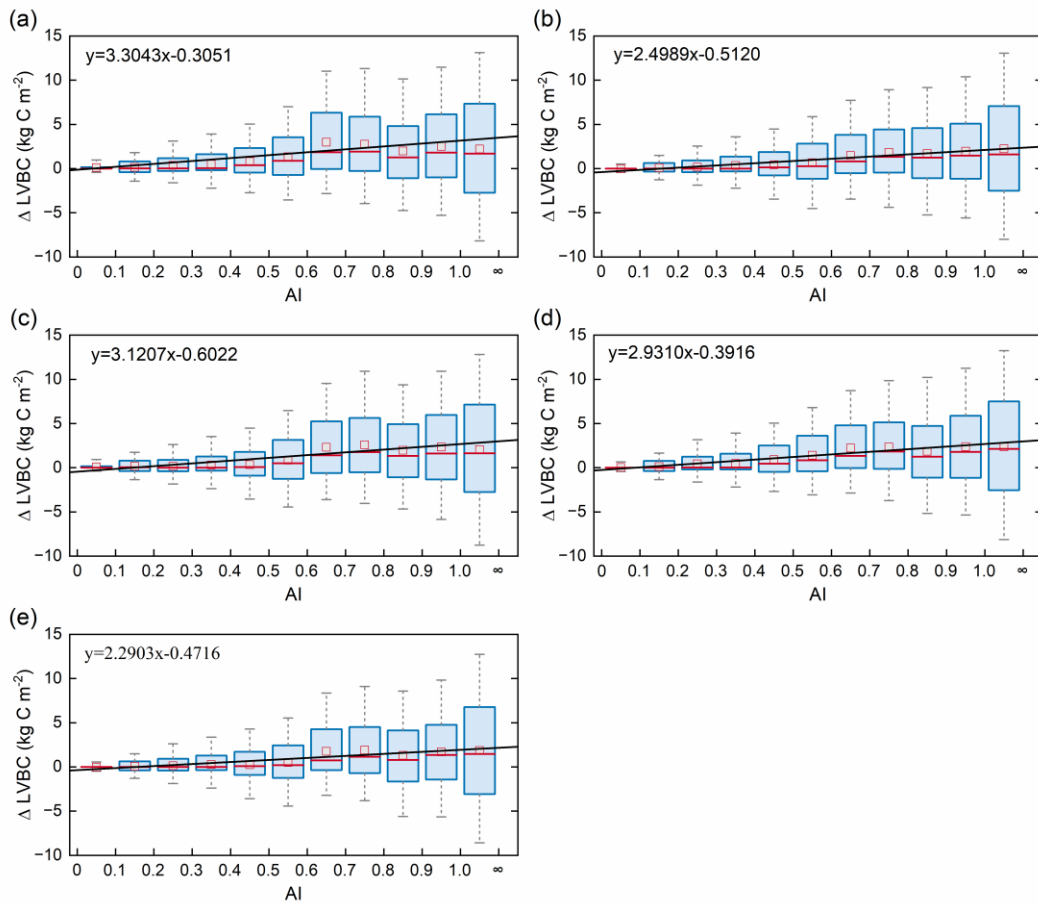
Figure 9. Relationships ~~in~~ of **the incremental change between AI and LVBC** ~~over the hydrological grid cells (Figure 1)~~. Magnitude of change in LVBC in the historical scenario S1 (a), CO_2 in scenario S2 (b), CO_2 + precipitation in scenario S3 (c), CO_2 + temperature in scenario S4 (d), and CO_2 + radiation in scenario S5 (e). ~~Range~~ The range of the box is 25%-75% of values; the range of the whiskers is 10%-90% of values; the small red square is average value; the red line is the median line; and the black line is the fitted curve. Positive value of the Y axis represents the magnitude of increased LVBC from 1916 to 2015 under water-limitations conditions, and vice versa. AI of grid cells is calculated by multiyear average precipitation and multiyear average potential evapotranspiration in the period of 1916-2015. Categories of hydrological zones include: hyper-arid (AI ≤ 0.05), arid (0.05 < AI ≤ 0.2), semi-arid (0.2 < AI ≤ 0.5), sub-humid (0.5 < AI ≤ 0.65), and humid (AI > 0.65).

467   Terrestrial water availability emerged as a key regulator of terrestrial carbon storage, by affecting the

468   response mechanism of the vegetation carbon stock to changes in driving factors. As shown in Figures 9

469   and 10, with the accumulated change of LVBC and WVBC in the period of 1916 to 2015 across the

470   aridity index (i.e., an increase in available water), the magnitude and range in responses of LVBC density

24

471 and WVBC density gradually increase. Based on the results of the historical simulation (Figure 9), we

472 find a positive relationship between LVBC and aridity index. In extreme water stress, the increase of

473 LVBC tends to zero and plants stop increasing their carbon storage. There is no obvious difference in

474 the slopes of fitting curves between factorial simulations, which shows the robustness in the response of

475 LVBC to the change of water stress. The pattern of the enhanced magnitude and range of variation in the

476 WVBC density is unimodal with water stress gradient in all factorial simulations. With the increasing of

477 AI, the magnitude of change in WVBC increases at first and then decreases finally. The mitigation of

478 water stress promotes WVBC increase, while excess surface water limits the response of WVBC to

479 changes in climate and CO_2. These results reveal that the carbon stock increases stimulated by changes

480 in climate and CO_2 are constrained by water available. With increased warming, water limitations are

481 expected to increasingly limit the carbon stock increase, specially at arid regions. To further reveal the

482 controls of water limitation on the responses of inner carbon storages to each driver, we analyse the long-

483 term variability of potential vegetation carbon stocks by means of factorial simulations for each

484 hydrological region (Figure 1). Figure A7b shows that the ~~maximum change magnitude~~fluctuation range

485 (the difference between maximum value and minimum value in each factorial simulation) of LVBC

486 density across all factorial simulation is 1.202 kg C m^{-2} in the hyper-arid regions for the 1916-2015

487 period. As shown in Figure A7f, the ~~maximum change magnitude~~fluctuation range of LVBC density in

488 humid regions is 6.068 kg C m^{-2} during the same period. In Figure A8b, the maximum change

489 magnitude of WVBC density across all factorial simulation is 0.011 kg C m^{-2} in the hyper-arid regions

490 during the time of 1916-2015. In Figure A8f, the maximum change magnitude of WVBC density is 0.046

491 kg C m^{-2} in humid regions during the same period. Compared with plants ~~lived~~ in arid~~ity~~ regions, plants

492 in humid regions show more dramatic responses to the stimulation from drivers' change. With a lessening

493 of water stress (from hyper-arid to humid region), the response magnitudes of the carbon stock to the

494 changes of climate and CO_2 gradually become more noticeable. The robust pattern in the zonal average

495 density of the carbon stock shows that terrestrial water limitations strongly regulate the enhanced
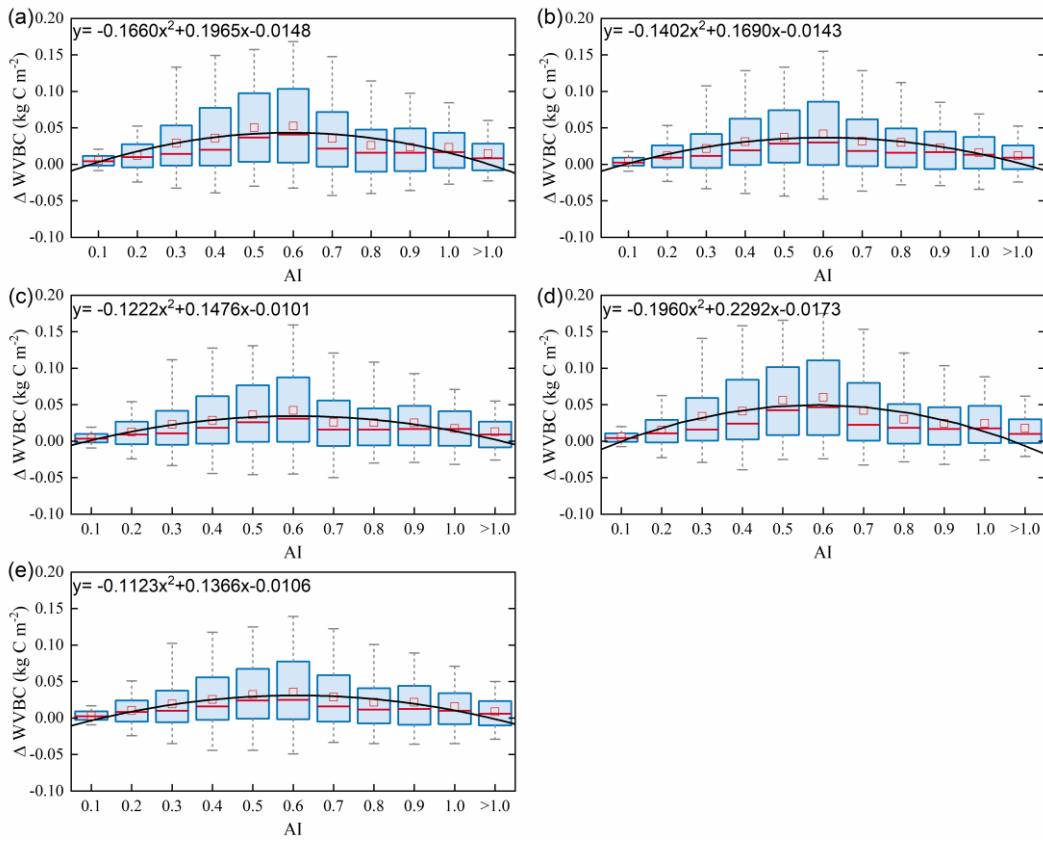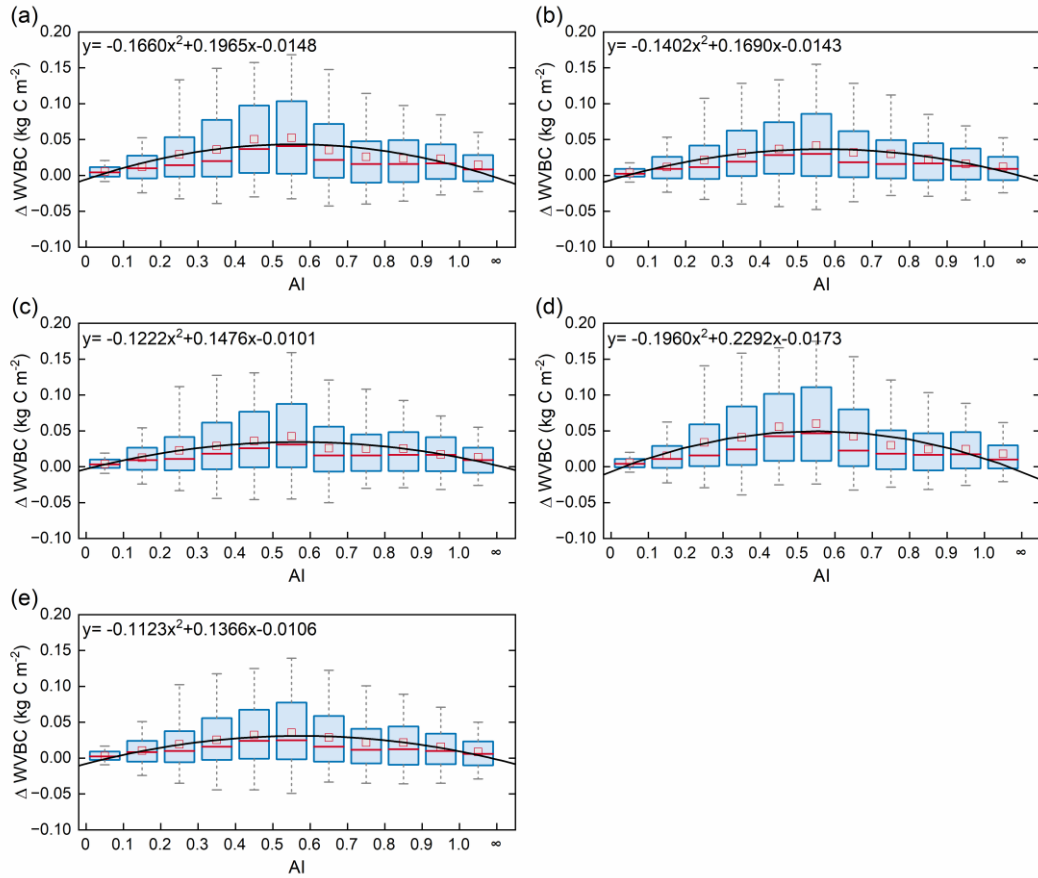
496 magnitude of the carbon stock.

Figure 10. Relationships ~~in~~ of the incremental change in AI and WVBC ~~over the hydrological grid cells (Figure 1)~~. Magnitude of change in WVBC in the historical scenario S1 (a), CO_2 in scenario S2 (b), CO_2 + precipitation in scenario S3 (c), CO_2 + temperature in scenario S4 (d), and CO_2 + radiation in scenario S5 (e). The ~~R~~range of the box is 25%-75% of values; the range of the whiskers is 10%-90% of values; the small red square is average value; the red line is the median line, and the black line is the fitted curve. Positive value of the Y axis represents the magnitude of increased WVBC from 1916 to 2015 under water-limitations conditions, and vice versa. AI of grid cells is calculated by multiyear average precipitation and multiyear average potential evapotranspiration in the period of 1916-2015. Categories of hydrological zones include: hyper-arid (AI $\leq$ 0.05), arid (0.05 < AI $\leq$ 0.2), semi-arid (0.2 < AI $\leq$ 0.5), sub-humid (0.5 < AI $\leq$ 0.65), and humid (AI > 0.65).

497   Water limitations not only directly reduced the magnitude of the response in the two fractions' carbon

498   stock (LVBC and WVBC) to changes in climate and CO_2, but also indirectly confined the response

499   direction of each fractions' carbon stock by transforming vegetation structure and function. Figure 11

500   illustrates temporal variations in the carbon stock ratio within and between hydrological regions. From

501   hyper-arid ~~zones~~ regions to humid ~~zones~~regions, the fluctuation range ~~(the difference between maximum~~

502   ~~value and minimum value in each factorial simulation)~~ of LVBC/WVBC ratio significantly changes. The

503   fluctuation magnitudes of LVBC/WVBC in humid and hyper-arid ~~zones~~ regions are greater than that in

504   other hydrological ~~zones~~regions. Compared with plants in hyper-arid ~~zones~~regions, plants in humid

505   ~~zones~~ regions exhibit more significant responses to changes in climate and CO_2. Meanwhile, the long-

506   term effects of driver changes have a remarkable influence on this carbon allocation pattern at global

507   level (Figure 7d). Under the synergistic effect of drivers and water stress, the trends of light- and water-

508   gathering vegetation carbon stock are upward in the past hundred years (Figure 6). However, there is a

509   difference in the increasing rate between LVBC and WVBC, resulting in a dramatic and complicated

510   fluctuation in global LVBC/WVBC ratio (Figure 11a). Whereas LVBC decreases and WVBC increases

511   in hyper-arid and arid regions (Fig. A7 and A8), causing a downward trend in LVBC:WVBC ratio,

512   semiarid regions see an increase in LVBC. ~~The density of LVBC decreases and that of WVBC increases~~

513   ~~in hyper-arid and arid zones for all factorial simulations (Figures A7 and A8).~~ So, the ratio of LVBC and

514   WVBC shows a downward trend in these ~~zones~~regions. LVBC in semi-arid regions shows upward

515   tendency in the past years (Figure A7d) because of the aridity mitigation. There is an upward trend in

516 WVBC in semi-arid regions (Figure A8d). Plants in semi-arid regions still utilize a tolerance strategy

517 and allocates more non-structural carbon to water-gathering vegetation organ to resist water stress,

518 resulting in the decline of LVBC/WVBC ratio. In humid ~~zones~~regions, light- and water-gathering

519 biomass carbon stocks both increased ~~in all factorial simulations~~ (Figures A7 and A8). The proportion

520 of LVBC increases more than that of WVBC for capturing more resources like CO_2 and radiation energy,

521 leading to an increase in the LVBC/WVBC ratio. The value of LVBC/WVBC in S3 is higher than that

522 in S4 and S5, which represents that precipitation makes more contributions to the change of
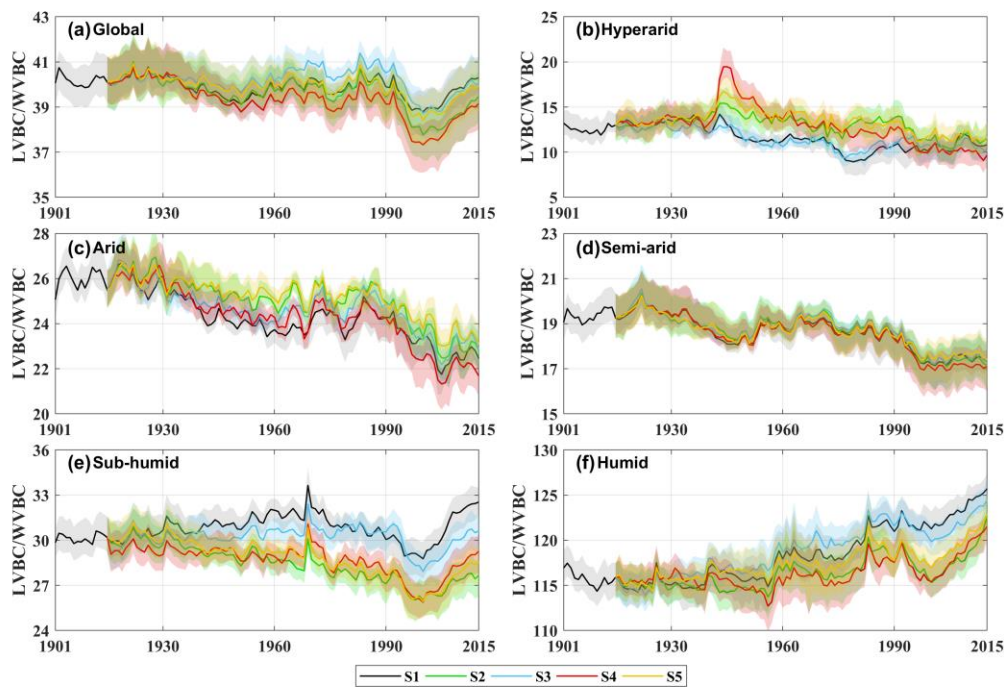
523 LVBC/WVBC ratio among meteorological factors.

Figure 11. Temporal fluctuations in carbon stock dynamics in vegetation biomass in different factorial simulations. Black indicates historical factorial simulation from 1901-2015, green indicates the CO_2-driven factorial simulation, blue indicates the precipitation-driven factorial simulation, red indicates the temperature-driving factorial simulation and yellow indicates radiation driven factorial simulation. Uncertainty bounds are provided as shaded areas reflect the intra-annual fluctuation (± 1 s.d.) (**a**) Modelled trend of LVBC/WVBC ratio in Global area. (**b-f**) Modelled trend of the LVBC/WVBC ratio in different hydrological regions (Figure 1).

4 Discussions and conclusion

To understand the response of carbon storage potential and its inner biomass carbon stocks to environmental change, we conducted a series of factorial simulations using SEIB-DGVM V3.02. More importantly, we investigated the extent of the responses of carbon stocks to water limitations.

Over the past 100 years, there has been an ongoing increase in the carbon storage capacity of the terrestrial ecosystem from 735 Pg C in 1916 to 855 Pg C in 2015 (Figure 6), which has slowed the rate at which atmospheric CO_2 has increased and may have mitigated global warming. These findings are consistent with the conclusions of research conducted at the local scale. For example, based on carbon flux data, Erb et al. (2008) suggested that the vegetation carbon stock in Austria increased from 1043 Mt C to 1249 Mt C (aboveground carbon stocks growth was 1.059 Mt C yr^{-1} and belowground carbon stocks growth was 0.2 Mt C yr^{-1}) since industrialization. Le Noë et al. (2020) showed that increases in the carbon stocks and carbon density were the predominant drivers in the forest terrestrial carbon sequestration capacity in France from 1850 to 2015. Tong et al. (2020) also found a substantial increase of aboveground carbon stocks in southern China (0.11 Pg C yr^{-1}) during the period 2002–2017. However, these studies focused on zonal trends in total vegetation carbon stocks and did not investigate the extent of the response in vegetation carbon stocks partitioned between light- and water-gathering biomass. Our results show that the increase in carbon stock in light-gathering vegetation organs was much larger than that in water-gathering vegetation organs, and light-gathering biomass carbon stock dominates the historical trend of the terrestrial carbon stock. During the past decades, the global land surface has been greening because of the flux and storage of more carbon into plant trunks and foliage (Zhu et al., 2016). LVBC increases 116.18 ± 2.34 Pg C from 1916 to 2015, accounting for 97.42% of the total carbon stock increase (119.26 ± 2.44 Pg C). The long-term trends and spatial pattern of vegetation carbon stock ~~are~~ predominated the variability characteristic of LVBC. The latitudinal bands of increasing annual change in LVBC are mainly distributed in tropical latitudes, a conclusion consistent with prior knowledge that tropical zones dominate carbon uptake and storage (Erb et al., 2018; Schimel et al., 2015). ~~Under the influences of environmental stressors, WVBC increases significantly in boreal latitudes.~~ Biomass carbon allocation between light- and water-gathering vegetation organs reflect the changes in individual growth, community structure and ecosystem function, which are important attributes in the investigation of

carbon stocks and carbon cycling within the terrestrial biosphere (Hovenden et al., 2014; Fang et al.,

2010; Ma et al., 2021). During the past hundred years, the ratio of LVBC/WVBC showed a slight upward

trend since LVBC increased relatively more ~~dramatically~~ than WVBC. The rate of increase is 0.0171

yr^{-1}, which is significant at the 0.01 level. To better absorb CO_2 and sunlight required for photosynthesis,

vegetated regions are gradually covered by vegetation with higher plant height and wider leaf area,

thereby adjusting their characteristic ecosystem functions (Erb et al., 2008).

Based on our factorial simulations (Figure 8), the influences of CO_2 fertilization induce the most

significant variation of the vegetation carbon stock. In addition, the responses of carbon stocks to the

changes of climatic factors are obvious, particularly at the ~~zonal~~ grid cell scale. Previous studies have

pointed out that the variation of the terrestrial carbon stock caused by releasing or sequestering carbon is

sensitive to anomalous changes in water availability and light use efficiency (Madani et al., 2020;

Humphrey et al., 2018). ~~At the grid cell scale, shown in Figure 8b and 8d, radiation and precipitation~~

~~dominate the long-term trend of carbon stocks over one third of global grid cells. At the global scale,~~

~~radiation and precipitation explain approximately 10% of long-term trend in LVBC and WVBC (Figure~~

~~8a and 8c). LVBC and WVBC variations driven by precipitation and radiation are ultimately offset by~~

~~spatially compensatory effects, which dampens the response of the carbon stock to these factors at global~~

~~scale (Jung et al., 2017). This spatially compensatory effect of climate changes is consistent with previous~~

~~analyses (Zhu et al., 2016) that climate changes explain 8% of the increasing carbon storage of global~~

~~foliage, while climate changes dominate the greening trend over 28.4% of the global land. Results reveal~~

~~that trends in temperature drove historical long-term trends in the potential carbon stocks, with faster~~

~~increases and considerable variation occurring by zone. The accumulated influence of climate warming~~

~~induces dramatic changes in the carbon stock at a global scale. Thus, we suggest that temperature~~

~~dominates the long-term trends in the carbon stock among climatic drivers, while a compensatory effect~~

~~exists in the global change in the carbon stock induced by precipitation and radiation.~~At the grid cell

scale, as shown in Figures 8b and 8d, temperature, radiation, precipitation, and other climate factors

(humidity and wind speed) dominate the long-term trend of carbon stocks over two thirds of global grid

cells. At the global scale, climate factors explain 17.55% and 10.72% of long-term trend in LVBC and

WVBC, respectively (Figures 8a and 8c). LVBC and WVBC variations driven by climate factors are

ultimately offset by spatially compensatory effects, which dampens the response of the carbon stock to

583 these factors at the global scale (Jung et al., 2017). Thus, contributions of precipitation and radiation to

584 the variability of LVBC and WVBC are relatively low at the global scale, and the effects of humidity

585 and wind speed on global carbon stock are minor. This spatially compensatory effect of climate changes

586 is consistent with a previous analysis (Zhu et al. 2016) which found that climate changes explain only 8%

587 of the increasing trend in foliage carbon storage at the global level but that they dominate the trend over

588 28.4% of global land area. Results show that trends in temperature drive historical long-term trends in

589 the potential carbon stocks, with faster increases and considerable variation occurring by grid cell. Thus,

590 our results reveal that temperature dominates the long-term trends of carbon stock among climatic drivers,

591 while a relatively strong compensatory effect exists in the global change in the carbon stock induced by

592 precipitation, radiation, humidity, and wind speed.

593

594 By partitioning the trends of LVBC and WVBC into five hydrological regions (Figure 1), we found that

595 the long-term change in carbon stocks is tightly coupled to terrestrial water availability. These results

596 indicate that vegetation in humid regions is responsible for most of the trend in global LVBC, while

597 plants in semi-arid regions play a dominate global role in controlling the long-term trend in WVBC

598 (Figures 9 and 10). As water stress decreases, the magnitude and range in variation of LVBC gradually

599 increase (Figure 9), which suggests that limited water availability constrains the response magnitude of

600 the changes in LVBC to changes in CO_2 and climate. The response pattern of WVBC growth to the

601 increasing water availability is different from that of LVBC. Drought mitigation promotes the growth of

602 WVBC. In sub-humid and humid regions, plants face low water limitations and intensified light-

603 competition and have to invest as much non-structural carbon as possible into leaf and trunk. This

604 allocation scheme leads to the decreased investment of ΔWVBC in wet regions. The result is consistent

605 with previous finding that plants reduce investment to roots in dense forests where aboveground

606 competition for light is high (Ma et al. 2021). Moreover, we found that indirect effects of water limitation

607 regulate increasing rate of each carbon pool. Although vegetation carbon stocks dramatically increase

608 under the effects of climate and CO_2 changes, the increasing rate of LVBC faster than WVBC in humid

609 regions. Vegetation stores more biomass in aboveground plant organs (trunk and foliage) to gather light.

610 Dryland plants decrease the LVBC/WVBC ratios and store more biomass below ground to enhance the

611   capture of water resources. Based on these results, we demonstrate that water limitations controlled the

612   variable response of terrestrial vegetation carbon stocks.

613

614   Our findings are consistent with other reports about the impact of increasing water limitations on

615   terrestrial ecosystem. Based on observation from satellite remote sensing observations, Madani et al.

616   (2020) found that the constraining impact of water limitation determines whether global ecosystem

617   productivity responds positively or negatively to the changes in climate factors. Madani et al. (2020)

618   found that changes in water constraints significantly affect the response patterns of ecosystem

619   productivity and net carbon exchange. Humphrey et al. (2021) found that increasing water stress limits

620   the response magnitude of carbon uptake rates through a down-regulation of stomatal conductance and

621   suggested that land carbon uptake is driven by temperature and vapour pressure deficit effects that are

622   controlled by terrestrial water availability. Ma et al. (2021) found that plants increase investment into

623   building roots in arid region because the extent of water limitation there is exacerbated by global warming.

624   Terrestrial hydrological conditions significantly affect the carbon cycle process of terrestrial ecosystems,

625   including carbon uptake, allocation, and stock. Terrestrial ecosystems utilize sensitive strategies to

626   allocate and store biomass to adjust to local hydrological conditions. A significant conclusion is that

627   water constraints not only confine the responses of vegetation carbon stocks to drivers of variability, but

628   also constrain the proportion of biomass carbon stocks in gather- and water-gathering fractions.

629

630   Distinguishing the response of carbon stock fractions estimated by SEIB-DGVM improves the

631   understanding of the interactive impacts of terrestrial carbon and water dynamics. However, uncertainty

632   still exists because of the limitations in the processes of modelling vegetation metabolism with SEIB-

633   DGVM. Trunk biomass contains tree branches and structural roots (coarse roots and tap roots) (Sato et

634   al., 2007), so the R/S ratio of potential vegetation in factorial simulations is smaller than the R/S of actual

635   vegetation in observation stations. Root biomass only contains the fine root biomass, leading to an

636   apparent underestimate in belowground organ biomass of trees and grasses compare with previous

637   conclusion (Ma et al., 2021; Yang et al., 2009). Availability of nitrogen is a key limiting factor for

638   vegetation growth, especially when higher CO_2 fertilization effects exist (Tharammal et al., 2019). The

639   limitation could be alleviated by nitrogen deposition in most temperate and boreal ecosystems. The

640 SEIB-DGVM experiments were conducted with a focus on documenting CO_2 fertilization and climate

641 change interactions; these experiments did not consider the influences of nitrogen deposition, which ~~leads~~

642 ~~to a slight~~ should cause an underestimate of the contributions of CO_2 fertilization on biomass production.

643

644 In summary, we evaluated SEIB-DGVM V3.02 and used this model to offer new perspectives on the

645 response of vegetation carbon storage potential to changes in climate and CO_2. Our simulation results

646 show that changes in CO_2, rather than climate, dominate the light- and water-gathering partitioning of

647 the carbon storage potential. More importantly, we suggest that the impact of CO_2 fertilization and

648 temperature effects on vegetation carbon-sequestration potential depends on water availability and its

649 impacts on plant stress. With increased global warming, water limitations are expected to increasingly

650 confine global carbon sequestration and storage. Our findings highlight the need to account for terrestrial

651 water limitation effects when estimating the response of the terrestrial carbon storage capacity to global

652 climate change, and the need for stronger interactions between those involved in vegetation model

653 development and those in between the hydrological and ecological research communities.

654 **Appendices**

655

<div align="center">Table A1. MCD12C1 legend and class descriptions</div>

| Name	Value	Description
Evergreen Needleleaf Forests	1	Dominated by evergreen conifer trees (canopy >2m). Tree cover >60%.
Evergreen Broadleaf Forests	2	Dominated by evergreen broadleaf and palmate trees (canopy >2m). Tree cover >60%.
Deciduous Needleleaf Forests	3	Dominated by deciduous needleleaf (larch) trees (canopy >2m). Tree cover >60%.
Deciduous Broadleaf Forests	4	Dominated by deciduous broadleaf trees (canopy >2m). Tree cover >60%.
Mixed Forests	5	Dominated by neither deciduous nor evergreen (40-60% of each) tree type (canopy >2m). Tree cover >60%.
Closed Shrublands	6	Dominated by woody perennials (1-2m height) >60% cover.
Open Shrublands	7	Dominated by woody perennials (1-2m height) 10-60% cover.
Woody Savannas	8	Tree cover 30-60% (canopy >2m).
Savannas	9	Tree cover 10-30% (canopy >2m).
Grasslands	10	Dominated by herbaceous annuals (<2m).
Permanent Wetlands	11	Permanently inundated lands with 30-60% water cover and >10% vegetated cover.
Croplands	12	At least 60% of area is cultivated cropland.
Urban and Built-up Lands	13	At least 30% impervious surface area including building materials, asphalt, and vehicles.
Cropland/Natural Vegetation Mosaics	14	Mosaics of small-scale cultivation 40-60% with natural tree, shrub, or herbaceous vegetation.
Permanent Snow and Ice	15	At least 60% of area is covered by snow and ice for at least 10 months of the year.
Barren	16	At least 60% of area is non-vegetated barren (sand, rock, soil) areas with less than 10% vegetation.
Water Bodies	17	At least 60% of area is covered by permanent water bodies.
Unclassified	255	Has not received a map label because of missing inputs

656
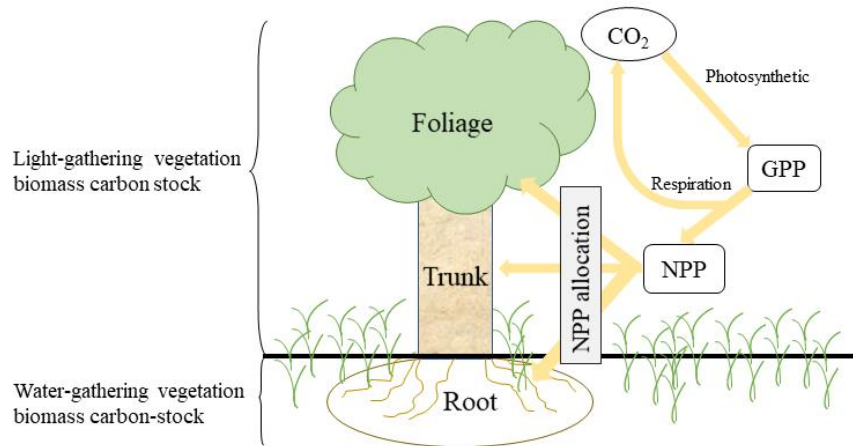
Figure A1. Schematic of ecosystem carbon cycle. Yellow arrow indicates carbon flux. Atmospheric CO_2 transitions into gross primary production (GPP) by photosynthesis. GPP is partitioned into respiration and net primary production (NPP). NPP is partitioned into three biomass carbon pools (foliage, trunk, and root).
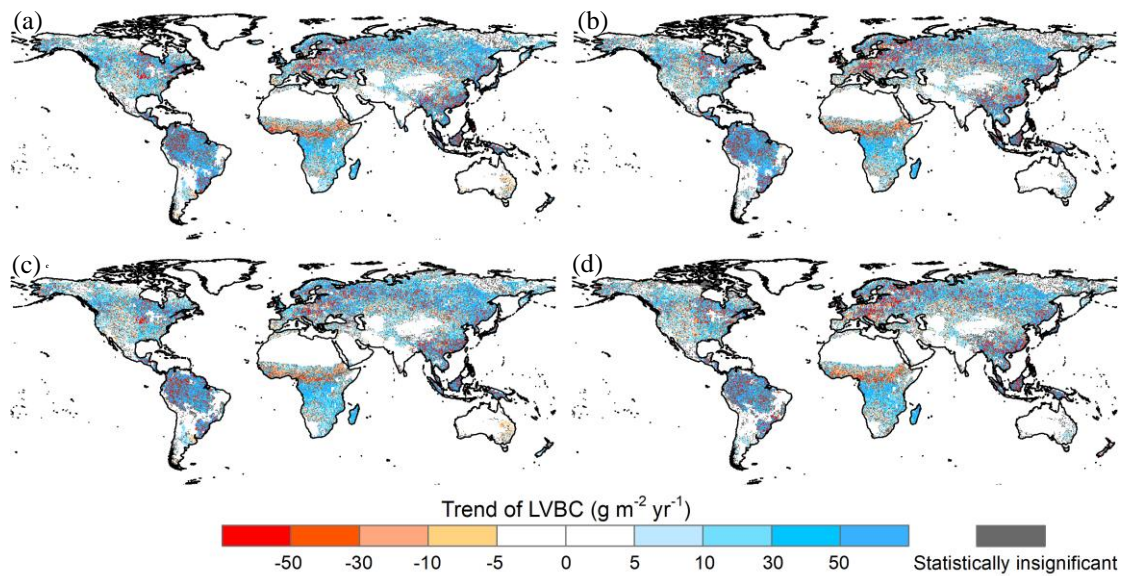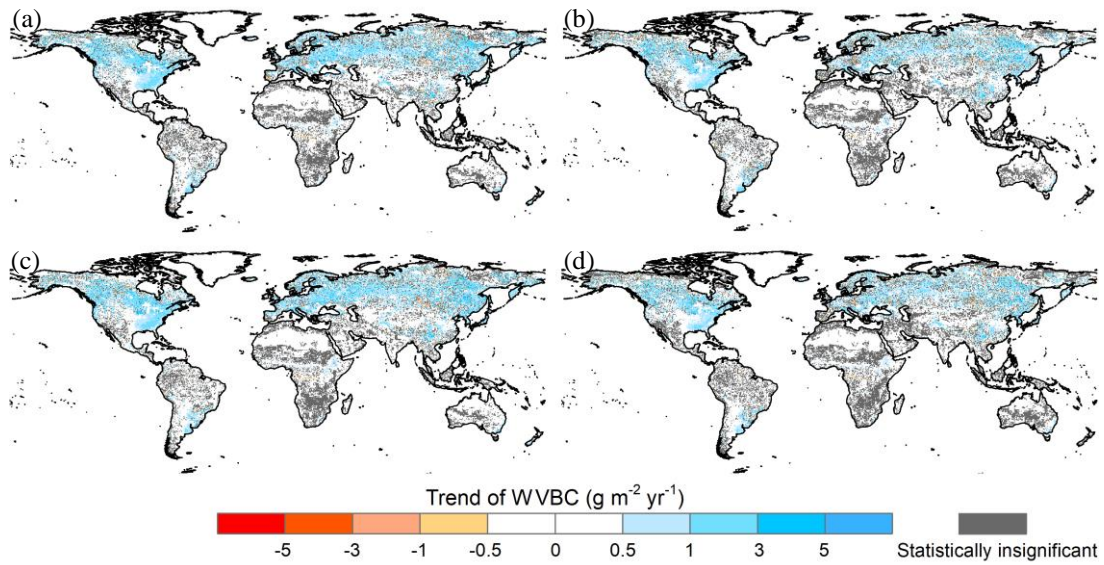
657

Figure A2. Potential LVBC trend maps during the period of 1916 to 2015 under different factorial simulations. (a) CO_2 driving factorial simulation (S2); (b) CO_2+precipitation driving factorial simulation (S3); (c) CO_2+temperature driving factorial simulation (S4); and (d) CO_2+radiation driving factorial simulation (S5). Positive values indicate increasing trends in the ratio, and vice versa. All results from Mann-Kendall and Sen's slope statistical tests correspond to the 95% confidence interval.

658

Figure A3. Potential WVBC variation trend maps during the period of 1916 to 2015 under different factorial simulations. (a) CO_2 driving factorial simulation (S2); (b) CO_2+precipitation driving factorial simulation (S3); (c) CO_2+temperature driving factorial simulation (S4); and (d) CO_2+radiation driving factorial simulation (S5). Positive values indicate increasing trends in the ratio, and vice versa. All results from Mann-Kendall and Sen's slope statistical tests correspond to the 95% confidence interval.

659
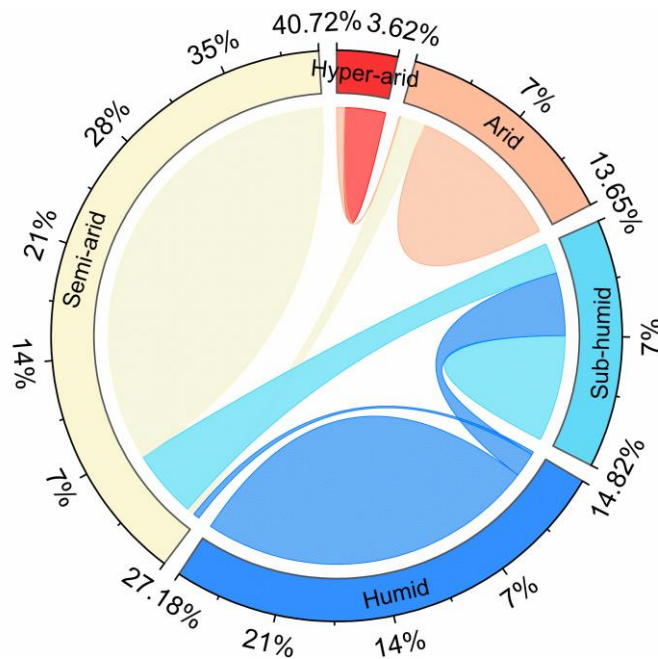
Figure A4. The shift of hydrological regions defined by the multiyear average AI index from the period of 1916-1945 to the period of 1986-2015. The outermost number represent the percentage of hydrological regions in 1916-1945.
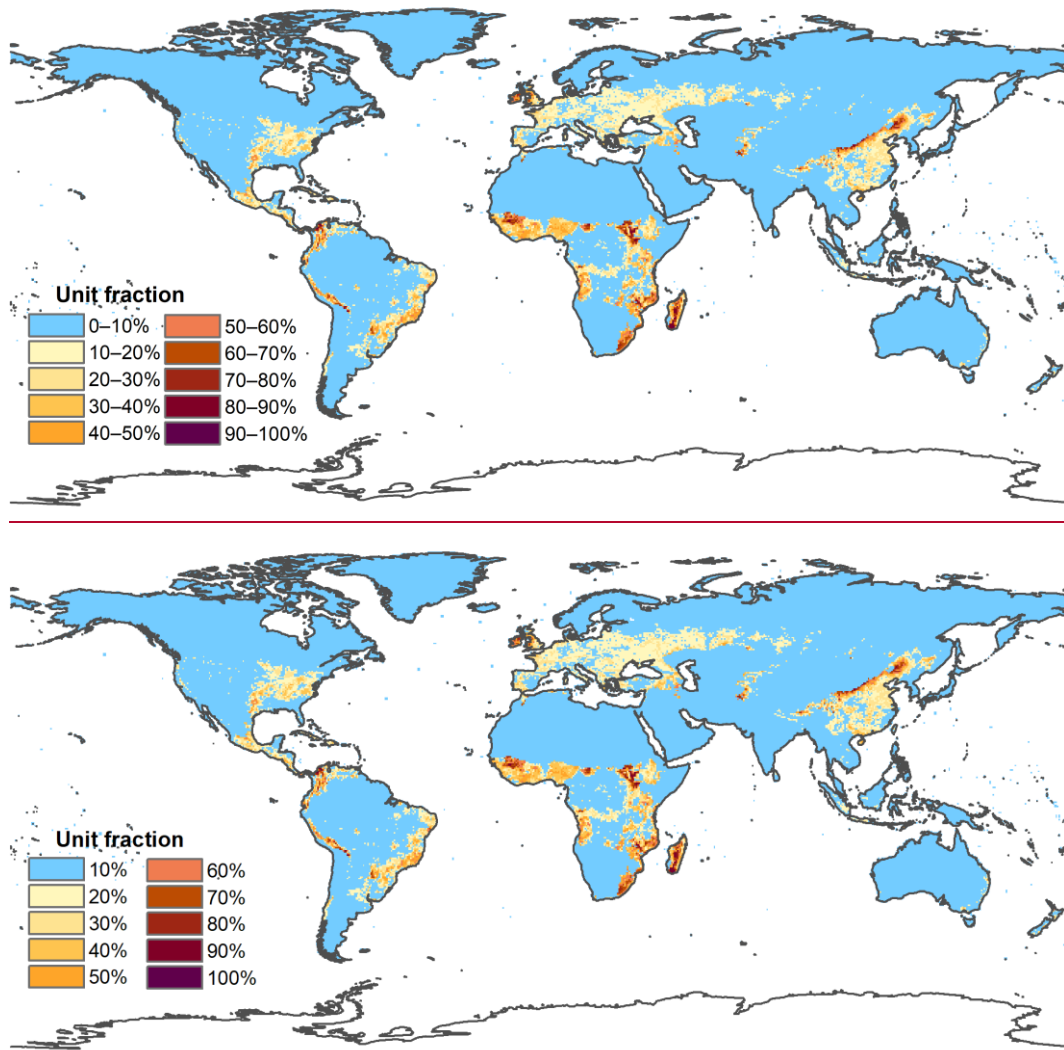
36

Figure A5. Spatial distribution of multi-year average fraction of managed pasture from 2001-2015 at 0.5×0.5 arc-degree resolution.
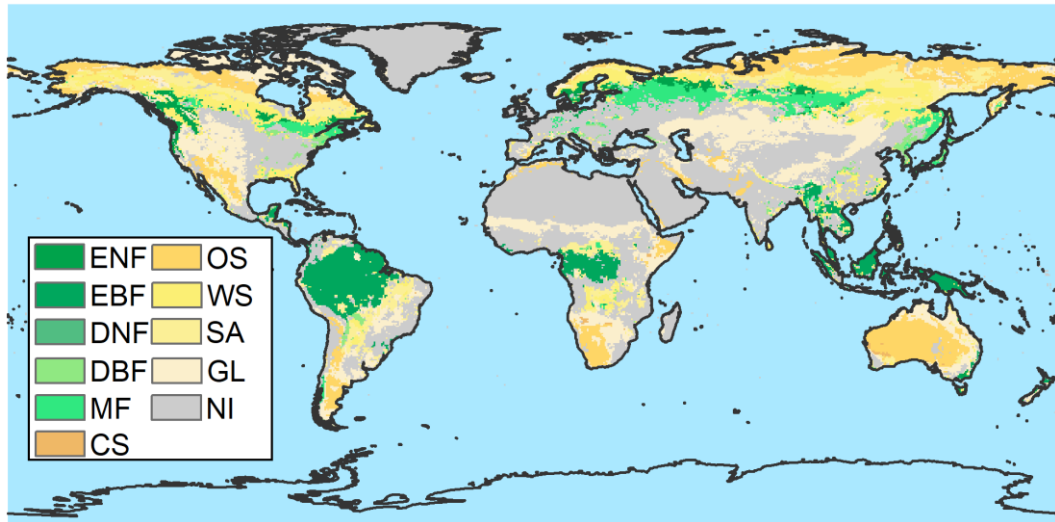
Figure A6. Map of grid cells whose largest vegetation componentland vegetation without anthropogenic disturbance from MCD12C1 and LUH2. ENF: Evergreen needleleaf forest, EBF: Evergreen broadleaf forest, DNF: Deciduous needleleaf forest, DBF: Deciduous broadleaf forest, MF: Mixed forest, CS: Closed shrublands, OS: Open shrublands, WS: Woody savannas, SA: Savannas, GL: Grasslands, NI: Not included, which means the zone is not covered by vegetation without anthropogenic disturbance.
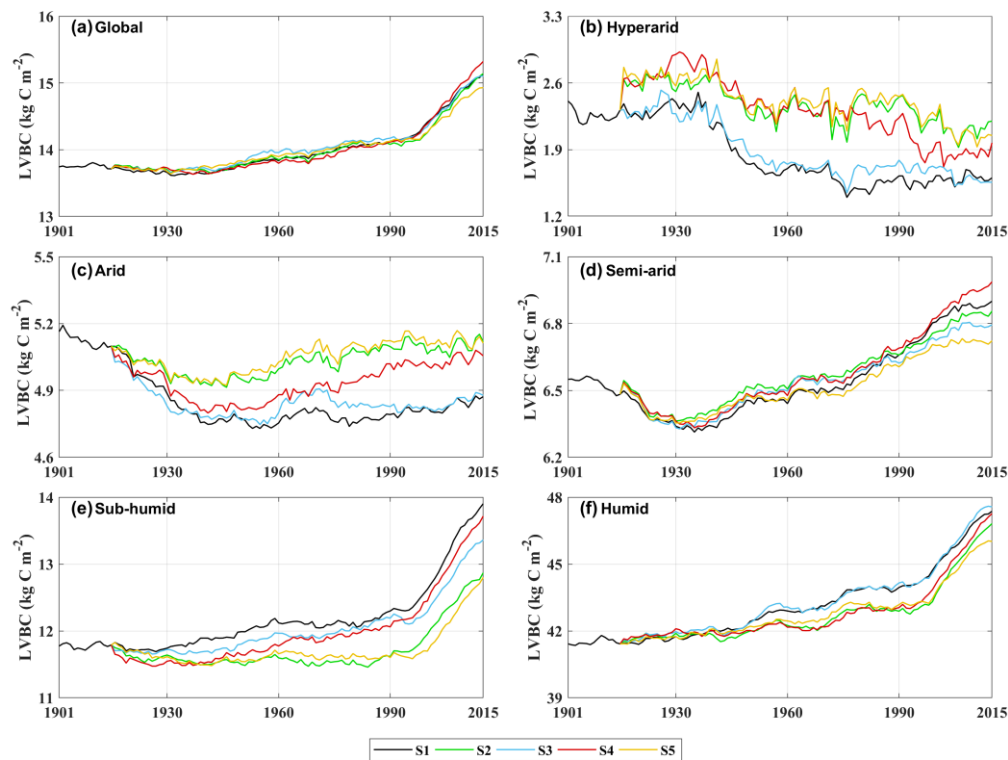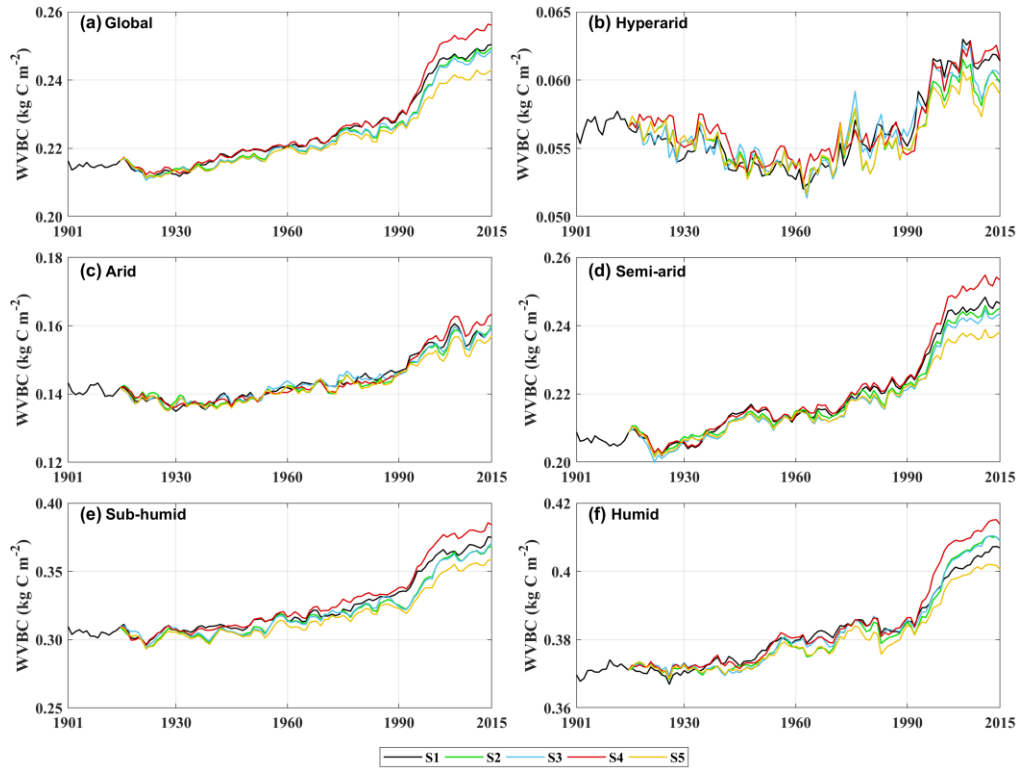
662

Figure A7. Trends in average density of potential LVBC. (a) Modelled trend of annual averaged LVBC globally. Modelled trends in annual averaged LVBC in hyper-arid ~~zone~~ region (b), arid ~~zone~~ region (c), semi-arid ~~zone~~ region (d), sub-humid ~~zone~~ region (e), and humid ~~zone~~ region (f).

663

Figure A8. Trends in average density of potential WVBC. (a) Modelled trend of annual averaged WVBC globally. Modelled trends in annual averaged WVBC in hyper-arid ~~zone~~ region (b), arid ~~zone~~ region (c), semi-arid ~~zone~~ region (d), sub-humid ~~zone~~ region (e), and humid ~~zone~~ region (f).

664 **Code and data availability statement**

665 The code of SEIB-DGVM version 3.02 can be download from http://seib-dgvm.com/. Climatic Research

666 Unit data can be downloaded from https://crudata.uea.ac.uk/cru/data/hrg/. The soil physical parameters

667 can be downloaded from www.iges.org/gswp. The reconstructed CO_2 concentration dataset and SEIB

668 code can be downloaded from http://seib-dgvm.com/. In model validation, Ecosystem Model-Data

669 Intercomparison (multiyear average NPP product) data were collected from

670 https://daac.ornl.gov/NPP/guides/NPP_EMDI.html. Remote sensing product MOD17A3 data were

671 obtained from https://lpdaac.usgs.gov/products/mod17a3hgfv006/, MCD12C1 data were obtained from

672   https://ladsweb.modaps.eosdis.nasa.gov/search/order, and LUH2 data were obtained from

673   https://luh.umd.edu/.

674   **Authors contributions**

675   T.S. designed research. T.S., and S.H. performed research and developed the methodology. T.S. analyzed

676   data and produced the outputs. T.S., S.H., C.J., and X.C. wrote the first manuscript draft. W.W. and W.G.

677   supervised the study. All the authors discussed the methodology and commented on various versions of

678   the manuscript.

679   **Competing interests**

680   The authors declare that they have no conflict of interest.

692 **References**

693 Ahlstrom, A., Raupach, M. R., Schurgers, G., Smith, B., Arneth, A., Jung, M., Reichstein, M., Canadell,
694   J. G., Friedlingstein, P., Jain, A. K., Kato, E., Poulter, B., Sitch, S., Stocker, B. D., Viovy, N., Wang,
695   Y. P., Wiltshire, A., Zaehle, S., and Zeng, N.: The dominant role of semi-arid ecosystems in the
696   trend and variability of the land CO_2 sink, Science, 348, 895-899, 10.1126/science.aaa1668, 2015.
697 Ajtay, G. L., Ketner, P., and Duvigneaud, P.: Terrestrial primary production and phytomass In: The
698   Global Cycle., Glob. Carbon Cycle, SCOPE, 129-181 pp.1979.
699 Bartholome, E. and Belward, A. S.: GLC2000: a new approach to global land cover mapping from Earth
700   observation data, Int J Remote Sens, 26, 1959-1977, 10.1080/01431160412331291297, 2005.
701 Bayer, A. D., Pugh, T. A. M., Krause, A., and Arneth, A.: Historical and future quantification of
702   terrestrial carbon sequestration from a Greenhouse-Gas-Value perspective, Global Environmental
703   Change, 32, 153-164, 10.1016/j.gloenvcha.2015.03.004, 2015.
704 Bazilevich, N. I., Rodin, L. Y., and Rozov, N. N.: Geographical Aspects of Biological Productivity,
705   Soviet Geograpgy Review and Translation, 5, 293-317 pp.1971.
706 Bloom, A. A., Exbrayat, J. F., van der Velde, I. R., Feng, L., and Williams, M.: The decadal state of the
707   terrestrial carbon cycle: Global retrievals of terrestrial carbon allocation, pools, and residence times,
708   Proceedings of the National Academy of Sciences of the United States of America, 113, 1285-1290,
709   10.1073/pnas.1515160113, 2016.
710 Chen, J., Ju, W., Ciais, P., Viovy, N., Liu, R. G., Liu, Y., and Lu, X. H.: Vegetation structural change
711   since 1981 significantly enhanced the terrestrial carbon sink, Nat Commun, 10, 4259,
712   10.1038/S41467-019-12257-8, 2019.
713 Chen, L.-P., Zhao, N.-X., Zhang, L.-H., and Gao, Y.-B.: Responses of two dominant plant species to
714   drought stress and defoliation in the Inner Mongolia Steppe of China, Plant Ecology, 214, 221-229,
715   10.1007/s11258-012-0161-y, 2013.
716 Cheng, L., Zhang, L., Wang, Y. P., Canadell, J. G., Chiew, F. H. S., Beringer, J., Li, L. H., Miralles, D.
717   G., Piao, S. L., and Zhang, Y. Q.: Recent increases in terrestrial carbon uptake at little cost to the
718   water cycle, Nat Commun, 8, 10.1038/s41467-017-00114-5, 2017.
719 Erb, K.-H., Gingrich, S., Krausmann, F., and Haberl, H.: Industrialization, Fossil Fuels, and the
720   Transformation of Land Use, Journal of Industrial Ecology, 12, 686-703, 10.1111/j.1530-
721   9290.2008.00076.x, 2008.
722 Erb, K.-H., Gaube, V., Krausmann, F., Plutzar, C., Bondeau, A., and Haberl, H.: A comprehensive global
723   5min resolution land-use data set for the year 2000 consistent with national census data, Journal of
724   Land Use Science, 2, 191-224, 10.1080/17474230701622981, 2007.
725 Erb, K.-H., Fetzel, T., Plutzar, C., Kastner, T., Lauk, C., Mayer, A., Niedertscheider, M., Körner, C., and
726   Haberl, H.: Biomass turnover time in terrestrial ecosystems halved by land use, Nat Geosci, 9, 674-
727   678, 10.1038/ngeo2782, 2016.
728 Erb, K.-H., Kastner, T., Plutzar, C., Bais, A. L. S., Carvalhais, N., Fetzel, T., Gingrich, S., Haberl, H.,
729   Lauk, C., Niedertscheider, M., Pongratz, J., Thurner, M., and Luyssaert, S.: Unexpectedly large
730   impact of forest management and grazing on global vegetation biomass, Nature, 553, 73-76,
731   10.1038/nature25138, 2018.
732 Fan, L., Wigneron, J. P., Ciais, P., Chave, J., Brandt, M., Fensholt, R., Saatchi, S. S., Bastos, A., Al-
733   Yaari, A., Hufkens, K., Qin, Y. W., Xiao, X. M., Chen, C., Myneni, R. B., Fernandez-Moran, R.,
734   Mialon, A., Rodriguez-Fernandez, N. J., Kerr, Y., Tian, F., and Penuelas, J.: Satellite-observed

735   pantropical carbon dynamics, Nat Plants, 5, 944-951, 10.1038/s41477-019-0478-9, 2019.

736 Fang, J., Yang, Y., Ma, W., Mohammat, A., and Shen, H.: Ecosystem carbon stocks and their changes
737   in China's grasslands, Science China. Life sciences, 53, 757-765, 10.1007/s11427-010-4029-x, 2010.

738 Friedlingstein, P., Joel, G., Field, C. B., and Fung, I. Y.: Toward an allocation scheme for global
739   terrestrial carbon models, Global Change Biol, 5, 755-770, DOI 10.1046/j.1365-2486.1999.00269.x,
740   1999.

741 Gentine, P., Green, J. K., Guérin, M., Humphrey, V., Seneviratne, S. I., Zhang, Y., and Zhou, S.:
742   Coupling between the terrestrial carbon and water cycles—a review, Environ Res Lett, 14, 083003,
743   10.1088/1748-9326/ab22d6, 2019.

744 Gill, R. and Jackson, R.: Global patterns of root turnover for terrestrial ecosystems, New Phytol, 147,
745   13-31, 10.1046/j.1469-8137.2000.00681.x, 2000.

746 Gocic, M. and Trajkovic, S.: Analysis of changes in meteorological variables using Mann-Kendall and
747   Sen's slope estimator statistical tests in Serbia, Global and Planetary Change, 100, 172-182,
748   10.1016/j.gloplacha.2012.10.014, 2013.

749 Gulbeyaz, O., Bond-Lamberty, B., Akyurek, Z., and West, T. O.: A new approach to evaluate the MODIS
750   annual NPP product (MOD17A3) using forest field data from Turkey, Int J Remote Sens, 39, 2560-
751   2578, 10.1080/01431161.2018.1430913, 2018.

752 Haberl, H., Erb, K. H., and Krausmann, F.: Human Appropriation of Net Primary Production: Patterns,
753   Trends, and Planetary Boundaries, Annu Rev Env Resour, 39, 363-391, 10.1146/annurev-environ-
754   121912-094620, 2014.

755 Harper, A. B., Wiltshire, A. J., Cox, P. M., Friedlingstein, P., Jones, C. D., Mercado, L. M., Sitch, S.,
756   Williams, K., and Duran-Rojas, C.: Vegetation distribution and terrestrial carbon cycle in a carbon
757   cycle configuration of JULES4.6 with new plant functional types, Geosci Model Dev, 11, 2857-
758   2873, 10.5194/gmd-11-2857-2018, 2018.

759 Harris, I., Osborn, T. J., Jones, P., and Lister, D.: Version 4 of the CRU TS monthly high-resolution
760   gridded multivariate climate dataset, Scientific Data, 7, 109, 10.1038/s41597-020-0453-3, 2020.

761 Hovenden, M. J., Newton, P. C., and Wills, K. E.: Seasonal not annual rainfall determines grassland
762   biomass response to carbon dioxide, Nature, 511, 583-586, 10.1038/nature13281, 2014.

763 Humphrey, V., Zscheischler, J., Ciais, P., Gudmundsson, L., Sitch, S., and Seneviratne, S. I.: Sensitivity
764   of atmospheric CO2 growth rate to observed changes in terrestrial water storage, Nature, 560, 628-
765   631, 10.1038/s41586-018-0424-4, 2018.

766 Humphrey, V., Berg, A., Ciais, P., Gentine, P., Jung, M., Reichstein, M., Seneviratne, S. I., and
767   Frankenberg, C.: Soil moisture–atmosphere feedback dominates land carbon uptake variability,
768   Nature, 592, 65-69, 10.1038/s41586-021-03325-5, 2021.

769 Hurtt, G. C., Chini, L. P., Frolking, S., Betts, R. A., Feddema, J., Fischer, G., Fisk, J. P., Hibbard, K.,
770   Houghton, R. A., Janetos, A., Jones, C. D., Kindermann, G., Kinoshita, T., Goldewijk, K. K., Riahi,
771   K., Shevliakova, E., Smith, S., Stehfest, E., Thomson, A., Thornton, P., van Vuuren, D. P., and
772   Wang, Y. P.: Harmonization of land-use scenarios for the period 1500-2100: 600 years of global
773   gridded annual land-use transitions, wood harvest, and resulting secondary lands, Climate Change,
774   109, 117-161, 10.1007/s10584-011-0153-2, 2011.

775 Hurtt, G. C., Chini, L., Sahajpal, R., Frolking, S., Bodirsky, B. L., Calvin, K., Doelman, J. C., Fisk, J.,
776   Fujimori, S., Goldewijk, K. K., Hasegawa, T., Havlik, P., Heinimann, A., Humpenöder, F.,
777   Jungclaus, J., Jed Kaplan, Kennedy, J., Kristzin, T., Lawrence, D., Lawrence, P., Ma, L., Mertz, O.,
778   Pongratz, J., Popp, A., Poulter, B., Riahi, K., Shevliakova, E., Stehfest, E., Thornton, P., Tubiello,

F. N., van Vuuren, D. P., Zhang, X.: Harmonization of Global Land-Use Change and Management for the Period 850-2100 (LUH2) for CMIP6, Geoscientific Model Development, 13, 5425-5464, 10.5194/gmd-13-5425-2020, 2021.

IPCC: Impacts, Adaptation and Vulnerability. Contribution of Working Group II to the Fourth Assessment Report of the Intergovernmental Panel on Climate Change, 2007.

Jung, M., Reichstein, M., Schwalm, C. R., Huntingford, C., Sitch, S., Ahlstrom, A., Arneth, A., Camps-Valls, G., Ciais, P., Friedlingstein, P., Gans, F., Ichii, K., Jain, A. K., Kato, E., Papale, D., Poulter, B., Raduly, B., Rodenbeck, C., Tramontana, G., Viovy, N., Wang, Y. P., Weber, U., Zaehle, S., and Zeng, N.: Compensatory water effects link yearly global land CO2 sink changes to temperature, Nature, 541, 516-520, 10.1038/nature20780, 2017.

Kaplan, J. O., Krumhardt, K. M., Ellis, E. C., Ruddiman, W. F., Lemmen, C., and Goldewijk, K. K.: Holocene carbon emissions as a result of anthropogenic land cover change, Holocene, 21, 775-791, 10.1177/0959683610386983, 2011.

Keenan, T. F., Prentice, I. C., Canadell, J. G., Williams, C. A., Wang, H., Raupach, M., and Collatz, G. J.: Recent pause in the growth rate of atmospheric CO2 due to enhanced terrestrial carbon uptake Nat Commun, 7, 10.1038/Ncomms16137, 2017.

Kindermann, G. E., Mcallum, I., Fritz, S., and Obersteiner, M.: A global forest growing stock, biomass and carbon map based on FAO statistics, Silva Fenn, 42, 387-396, 10.14214/Sf.244, 2008.

Le Noë, J., Matej, S., Magerl, A., Bhan, M., Erb, K. H., and Gingrich, S.: Modeling and empirical validation of long-term carbon sequestration in forests (France, 1850-2015), Glob Chang Biol, 26, 2421-2434, 10.1111/gcb.15004, 2020.

Liu, J., Bowman, K. W., Schimel, D. S., Parazoo, N. C., Jiang, Z., Lee, M., Bloom, A. A., Wunch, D., Frankenberg, C., Sun, Y., O'Dell, C. W., Gurney, K. R., Menemenlis, D., Gierach, M., Crisp, D., and Eldering, A.: Contrasting carbon cycle responses of the tropical continents to the 2015-2016 El Nino, Science, 358, eaam5690, 10.1126/science.aam5690, 2017.

Ma, H. Z., Mo, L. D., Crowther, T. W., Maynard, D. S., van den Hoogen, J., Stocker, B. D., Terrer, C., and Zohner, C. M.: The global distribution and environmental drivers of aboveground versus belowground plant biomass, Nat Ecol Evol, 5, 1110-+, 10.1038/s41559-021-01485-1, 2021.

Madani, N., Parazoo, N. C., Kimball, J. S., Ballantyne, A. P., Reichle, R. H., Maneta, M., Saatchi, S., Palmer, P. I., Liu, Z., and Tagesson, T.: Recent Amplified Global Gross Primary Productivity Due to Temperature Increase Is Offset by Reduced Productivity Due to Water Constraints, AGU Advances, 2, e2020AV000180, 10.1029/2020AV000180, 2020.

Magerl, A., Le Noë, J., Erb, K.-H., Bhan, M., and Gingrich, S.: A comprehensive data-based assessment of forest ecosystem carbon stocks in the U.S. 1907–2012, Environ Res Lett, 14, 125015, 10.1088/1748-9326/ab5cb6, 2019.

McConnaughay, K. D. M. and Coleman, J. S.: Biomass allocation in plants: ontogeny or optimality? A test along three resource gradients, Ecology, 80, 2581-2593, 10.1890/0012-9658(1999)080[2581:BAIPOO]2.0.CO;2, 1999.

Monteith, J. L. and Unsworth, M. H.: Principles of Environmental Physics, 2nd ed., London1990.

Olson, J., Watts, J., and Allison, L.: Carbon in Live Vegetation of Major World Ecosystems, Oak Ridge National Laboratory1983.

Pan, Y. D., Birdsey, R. A., Phillips, O. L., and Jackson, R. B.: The Structure, Distribution, and Biomass of the World's Forests, Annu Rev Ecol Evol S, 44, 593-622, 10.1146/annurev-ecolsys-110512-135914, 2013.

Pan, Y. D., Birdsey, R. A., Fang, J. Y., Houghton, R., Kauppi, P. E., Kurz, W. A., Phillips, O. L., Shvidenko, A., Lewis, S. L., Canadell, J. G., Ciais, P., Jackson, R. B., Pacala, S. W., McGuire, A. D., Piao, S. L., Rautiainen, A., Sitch, S., and Hayes, D.: A Large and Persistent Carbon Sink in the World's Forests, Science, 333, 988-993, 10.1126/science.1201609, 2011.

Piao, S. L., Friedlingstein, P., Ciais, P., Zhou, L. M., and Chen, A. P.: Effect of climate and CO2 changes on the greening of the Northern Hemisphere over the past two decades, Geophys Res Lett, 33, L23402, 10.1029/2006GL028205, 2006.

Piao, S. L., Wang, X., Wang, K., Li, X., Bastos, A., Canadell, J. G., Ciais, P., Friedlingstein, P., and Sitch, S.: Interannual variation of terrestrial carbon cycle: Issues and perspectives, Glob Chang Biol, 26, 300-318, 10.1111/gcb.14884, 2020.

Poorter, H.: Construction costs and payback time of biomass: a whole plant perspective, A Whole-Plant Perspective on Carbon-Nitrogen Interactions, SPB Academic Publishing, The Hague1994.

Poulter, B., Frank, D., Ciais, P., Myneni, R. B., Andela, N., Bi, J., Broquet, G., Canadell, J. G., Chevallier, F., Liu, Y. Y., Running, S. W., Sitch, S., and van der Werf, G. R.: Contribution of semi-arid ecosystems to interannual variability of the global carbon cycle, Nature, 509, 600-603, 10.1038/nature13376, 2014.

Prentice, I. C., Harrison, S. P., and Bartlein, P. J.: Global vegetation and terrestrial carbon cycle changes after the last ice age, New Phytol, 189, 988-998, 10.1111/j.1469-8137.2010.03620.x, 2011.

Roy, J., Saugier, B., and Mooney, H. A.: Estimations of global terrestrial productivity: converging toward a single number? In: Terrestrial Global Productivity, Academic Press, San Diego2001.

Ruesch, A. and Gibbs, H. K.: New IPCC Tier-1 global biomass carbon map for the year 2000, 2008.

Ryan, M. G.: Effects of Climate Change on Plant Respiration, Ecological Applications, 1, 157-167, 10.2307/1941808, 1991.

Sato, H., Itoh, A., and Kohyama, T.: SEIB–DGVM: A new Dynamic Global Vegetation Model using a spatially explicit individual-based approach, Ecological Modelling, 200, 279-307, 10.1016/j.ecolmodel.2006.09.006, 2007.

Sato, H., Kobayashi, H., Beer, C., and Fedorov, A.: Simulating interactions between topography, permafrost, and vegetation in Siberian larch forest, Environ Res Lett, 15, 095006, 10.1088/1748-9326/Ab9be4, 2020.

Saugier, B., Roy, J., and Mooney, H.: Estimations of Global Terrestrial Productivity, Terrestrial Global Productivity, Academic Press, San Diego, Calif2001.

Schimel, D., Stephens, B. B., and Fisher, J. B.: Effect of increasing CO2 on the terrestrial carbon cycle, Proceedings of the National Academy of Sciences of the United States of America, 112, 436-441, 10.1073/pnas.1407302112, 2015.

Seo, H. and Kim, Y.: Interactive impacts of fire and vegetation dynamics on global carbon and water budget using Community Land Model version 4.5, Geosci Model Dev, 12, 457-472, 10.5194/gmd-12-457-2019, 2019.

Shevliakova, E., Pacala, S. W., Malyshev, S., Hurtt, G. C., Milly, P. C. D., Caspersen, J. P., Sentman, L. T., Fisk, J. P., Wirth, C., and Crevoisier, C.: Carbon cycling under 300 years of land use change: Importance of the secondary vegetation sink, Global Biogeochem Cy, 23, 10.1029/2007gb003176, 2009.

Sun, F., Roderick, M. L., and Farquhar, G. D.: Changes in the variability of global land precipitation, Geophys Res Lett, 39, L19402, 10.1029/2012gl053369, 2012.

Tei, S., Sugimoto, A., Liang, M. C., Yonenobu, H., Matsuura, Y., Osawa, A., Sato, H., Fujinuma, J., and

867   Maximov, T.: Radial Growth and Physiological Response of Coniferous Trees to Arctic
868   Amplification, J Geophys Res-Biogeo, 122, 2786-2803, 10.1002/2016JG003745, 2017.
869   Terrer, C., Phillips, R. P., Hungate, B. A., Rosende, J., Pett-Ridge, J., Craig, M. E., van Groenigen, K. J.,
870   Keenan, T. F., Sulman, B. N., Stocker, B. D., Reich, P. B., Pellegrini, A. F. A., Pendall, E., Zhang,
871   H., Evans, R. D., Carrillo, Y., Fisher, J. B., Van Sundert, K., Vicca, S., and Jackson, R. B.: A trade-
872   off between plant and soil carbon storage under elevated CO2, Nature, 591, 599-603,
873   10.1038/s41586-021-03306-8, 2021.
874   Tharammal, T., Bala, G., Devaraju, N., and Nemani, R.: A review of the major drivers of the terrestrial
875   carbon uptake: model-based assessments, consensus, and uncertainties, Environ Res Lett, 14,
876   093005, 10.1088/1748-9326/Ab3012, 2019.
877   Tong, X. W., Brandt, M., Yue, Y. M., Ciais, P., Jepsen, M. R., Penuelas, J., Wigneron, J. P., Xiao, X.
878   M., Song, X. P., Horion, S., Rasmussen, K., Saatchi, S., Fan, L., Wang, K. L., Zhang, B., Chen, Z.
879   C., Wang, Y. H., Li, X. J., and Fensholt, R.: Forest management in southern China generates short
880   term extensive carbon sequestration, Nat Commun, 11, 10.1038/s41467-019-13798-8, 2020.
881   West, P. C., Gibbs, H. K., Monfreda, C., Wagner, J., Barford, C. C., Carpenter, S. R., and Foley, J. A.:
882   Trading carbon for food: Global comparison of carbon stocks vs. crop yields on agricultural land,
883   Proceedings of the National Academy of Sciences of the United States of America, 107, 19645-
884   19648, 10.1073/pnas.1011078107, 2010.
885   Wild, M., Gilgen, H., Roesch, A., Ohmura, A., Long, C. N., Dutton, E. G., Forgan, B., Kallis, A., Russak,
886   V., and Tsvetkov, A.: From dimming to brightening: Decadal changes in solar radiation at Earth's
887   surface, Science, 308, 847-850, 10.1126/science.1103215, 2005.
888   Yang, Y., Fang, J., Ma, W., Guo, D., and Mohammat, A.: Large-scale pattern of biomass partitioning
889   across China's grasslands, Global Ecology and Biogeography, 19, 268-277, 10.1111/j.1466-
890   8238.2009.00502.x, 2010.
891   Zhang, H., Song, T. Q., Wang, K. L., Yang, H., Yue, Y. M., Zeng, Z. X., Peng, W. X., and Zeng, F. P.:
892   Influences of stand characteristics and environmental factors on forest biomass and root-shoot
893   allocation in southwest China, Ecol Eng, 91, 7-15, 10.1016/j.ecoleng.2016.01.040, 2016.
894   Zhu, Z. C., Piao, S. L., Myneni, R. B., Huang, M. T., Zeng, Z. Z., Canadell, J. G., Ciais, P., Sitch, S.,
895   Friedlingstein, P., Arneth, A., Cao, C. X., Cheng, L., Kato, E., Koven, C., Li, Y., Lian, X., Liu, Y.
896   W., Liu, R. G., Mao, J. F., Pan, Y. Z., Peng, S. S., Penuelas, J., Poulter, B., Pugh, T. A. M., Stocker,
897   B. D., Viovy, N., Wang, X. H., Wang, Y. P., Xiao, Z. Q., Yang, H., Zaehle, S., and Zeng, N.:
898   Greening of the Earth and its drivers, Nat Clim Change, 6, 791-+, 10.1038/Nclimate3004, 2016.